Volume 4 FEBRUARY, 1933 Number 2

PHYSICS

A Journal of General and Applied Physics

Infrared Absorption Spectra of Certain Organic Compounds, Including the Principal Types Present in Gasoline

CHARLES F. KETTERING, *General Motors Research Laboratories* AND W. W. SLEATOR, *University of Michigan*

(Received October 25, 1932)

The absorption spectra for twenty-five compounds, of which seventeen are typical of the important components of gasoline and which include both chain and ring molecules, all in the vapor state, have been examined throughout the spectral range 1μ to 30μ, by using prisms of NaCl, KCl and KBr. The percentage absorption is shown graphically in the charts which follow as function of the wave-length for specified amounts of material. The curves indicate certain distinctive features characteristic of each different molecule, as well as bands common to several or all the compounds. The resolution was not sufficient to separate rotational lines in any of the bands. In addition to the hydrocarbons, eight other substances, tetraethyl lead (the only material studied in the liquid state), tetraethyl germanium, tetramethyl tin, and tetramethyl lead and also aniline, dicyclopentadiene, methyl nitrate and diethyl peroxide were investigated. They were included in the list on account of their influence upon the detonation of fuel in the gasoline engine.

INTRODUCTION

THE following paper presents the results of a series of absorption measurements which were carried out under the auspices of the Department of Engineering Research at the University of Michigan for the Research Laboratory of the General Motors Corporation. The materials examined include the types of hydrocarbons which make up the principal components of gasoline, and certain other materials the interest of which lies in their effect on the detonation or "knock" of fuels in the gasoline engine. In Table I the numbers refer to the charts giving the absorption data in graphical form.

TABLE I.

Material	Chart number	Material	Chart number
Cyclohexane	1	Aniline	13
Diiso butylene	2	Tetraethyl germanium	14
Normal hexane	3	Tetramethyl tin	15
2, 3 Dimethyl butane	4	Tetramethyl lead	16
Cyclohexene	5	Benzene	17
1 Hexene	6	Toluene	18
1 Octene	7	3 Heptene	19
Methyl cyclohexane	8	2 Methyl pentane	20
Normal pentane	9	2, 2, 4-Trimethyl pentane	21
Dicyclopentadiene	10	3 Methyl pentane	22
Gamma heptine	11	2, 2 Dimethylbutane	23
Diethyl peroxide	12	Tetraethyl lead	24
		Methyl nitrate	25

APPARATUS

Two different spectrometers were used in mapping the following spectra. The first was of the Wadsworth type, equipped with a 60° NaCl prism, mirrors 12 cm in diameter and of 50 cm focal length, and a thermopile constructed by Firestone.[1] The small thermopile case was evacuated by a mechanical pump and activated charcoal, and was joined to a Moll galvanometer of d'Arsonval type. The combination was sensitive enough so that, with slits as small as 0.1 mm, it was possible to get good deflections out to 4μ, and with slits at 0.5 mm out to 14μ, without a relay. At 6μ the slits were usually 0.2 mm wide, and this corresponds to a spectral range of 0.07μ. Deflections were observed on a translucent scale. After the angle of the prism had been measured, and the position was determined in which light, reflected from the first

[1] F. A. Firestone, *Radiation Thermopile Design*, Rev. Sci. Inst. **1**, 630 (1930).

face of the prism, returned to the entering slit, it was possible to compute the figures for a calibration curve from the indices of refraction for NaCl.[2]

For part of the work the recording spectrograph described by Randall and Strong[3] was available. This instrument was equipped first with a 30° prism of potassium chloride with a surface silvered by evaporation. With this arrangement it was possible to follow the spectra to 20μ. It was used instead of the Wadsworth spectrometer for some of the materials (as indicated on the charts), and nearly all the spectra were extended by it beyond the range of the rocksalt prism. The measurements were carried still further by the use of a potassium bromide prism of 60° in the same apparatus, then equipped with a stationary and a moving mirror. The indices of refraction of KBr are now available,[4] but the recording spectrometer was calibrated empirically by means of absorption bands of known wave-lengths, principally those of water vapor, carbon dioxide, ammonia, acetylene and the methyl halides. These wave-lengths have been determined in this laboratory by the use of gratings.[5] The absorption band of acetylene of 13.5μ was photographed on nearly every record in order to have a check on the calibration.

The absorption cell used with the Wadsworth spectrometer was provided with windows of NaCl for most of the work, but mica was used where suitable, and some spectra were taken with windows of cellulose, made by dropping a little lacquer on water and lifting off the resulting film. These windows, however, were very fragile and proved pervious to the lighter hydrocarbons.

With the self-recording spectrometer the absorption cell, which had bromide windows capable of withstanding pressure, was inside the exhausted case and was pumped out separately through a small metal tube. It was connected to a mercury manometer so that the pressure of the inclosed gas could be read directly. In most cases records were taken with several different pressures, as best brought out the details of the absorption. A flask containing the liquid hydrocarbon was sealed to a second metal tube leading to the absorption cell; and opening a stopcock permitted more or less evaporation into the evacuated cell.

With the Wadsworth spectrometer the absorption cell was not pumped out, but some of the liquid to be studied was exposed inside the cell so as nearly to saturate the space within. The absorbing effect of constituents of the air was eliminated by moving the cell into and out of the beam of radiation. With some of the heavier molecules it was necessary to heat the cell. This presented a difficulty, because the windows which were rocksalt plates were always a little cooler than the cell walls around which the heating coil was wound, and they collected a film of liquid. This was avoided by putting the material to be studied in a little cup or cistern outside the cell but opening into it. This cistern was five or ten degrees cooler than the cell which could be brought up to 150°C. With those materials which required the heated cell, of which dicyclopentadiene was one, the determination of the density of the vapor in the path of the radiation becomes an estimate, based on the boiling point of the material and on what is known about its change of vapor pressure with temperature. Unless otherwise specified on the charts, the absorption occurred in a cell 12 cm long.

A good deal of work has been done on the infrared spectra of hydrocarbons.[6] This work,

[2] These numbers, as determined by Paschen and others, are now accessible, with references to original sources, in *Das Ultrarote Spektrum*, Cl. Schaefer and F. Matossi, Springer, Berlin, pp. 45–47 (1930).

[3] H. M. Randall and John Strong, *A Self-Recording Spectrometer, Rev. Sci. Inst.* **2**, 585 (1931).

[4] E. Gundelach, *Die Dispersion von KBr Kristallen im Ultraroten*, Zeits. f. Physik **66**, 775 (1930).

[5] E. K. Plyler and W. W. Sleator, *Further Study of the Absorption of Infrared Radiation by Water Vapor*, Phys. Rev. **37**, 1493 (1931).

P. E. Martin and E. F. Barker, *The Infrared Absorption Spectrum of Carbon Dioxide.* Phys. Rev. **41**, 291 (1932).

E. F. Barker, *Molecular Spectrum of Ammonia; II, Double Band at* 10μ. Phys. Rev. **33**, 684 (1929).

Charles F. Meyer and Aaron A. Levin, *The Infrared Absorption Spectra of Acetylene, Ethylene and Ethane.* Proc. Nat. Acad. Sci. **13**, 298 (1927).

Willard H. Bennett and Charles F. Meyer, *Infrared Absorption Spectra of the Methyl Halides.* Phys. Rev. **32**, 888 (1928).

[6] Schaefer and Matossi, in *Das Ultrarote Spektrum*, in Article 33 (page 266) on the spectra of organic liquids and vapors, give a summary of the infrared absorption spectra

however, presents no systematic examination of the types of compounds present in gasoline, and with the exceptions noted the spectra are carried only through the very near infrared region. In fact, the work with relatively high dispersion is concerned largely with the absorption bands near 3μ, which seem to be shown by all hydrocarbons, and are taken to arise from variations in the single hydrogen-carbon separation. The charts given with this paper, while not characterized by high resolution, present the spectra of certain substances in the important region between 1 and 30μ. The charts themselves do not extend to 30μ, but no absorption bands (at wave-length less than 30μ) were found beyond the limits given, and if the hydrocarbons have any such absorption bands they are very weak. These spectra constitute a first step in the study of the molecular structure of the compounds considered, a study which might be carried further by the use of higher resolution. It is possible to compute in some cases what resolution will probably be necessary in order to observe the fine structure of the absorption bands. In the spectrum of cyclohexane, for example, there is a three part band with center of 14.85μ which has distinctly the appearance of a vibration-rotation band with a zero branch. The separation of the peaks of the P and R-branches, if such they are, is about 0.6μ so that

$$\Delta\nu = (3\times10^{14}\times0.6)/15^2 = 8\times10^{11}$$

vibrations per second. Assuming that the moment of inertia concerned in the production of this band is one of the two equal moments of inertia for a thin disk, it comes out from simple kinetic theory to be about 7×10^{-39} g cm^2. A better calculation as made by Dennison in work not yet published gives $I=14\times10^{-39}$ g cm^2. By using the latter value, the fine structure separation is expressed by the value of the frequency interval between successive lines as $\Delta\nu=1.2\times10^{10}$, or about 0.4 waves per cm. This is about 1/70 of the doublet separation. The very similar band of benzene at 9.5μ, where $\Delta\lambda$ is 0.25μ, gives almost the same moment of inertia. This band has been worked over with a combination prism and grating spectrometer. The theoretical resolving power of this spectrometer was such that the separation of the band into its combination lines appeared to be possible, but careful trials did not reveal any fine structure. If we assume the cyclohexane molecule to be essentially flat, the value $2I$ for the moment of inertia about an axis perpendicular to the plane gives the distance between neighboring carbon atoms as 1.4×10^{-8} cm.

The spectra shown in Figs. 1–25 suggest the possibility of a beginning in qualitative analysis of hydrocarbon mixtures by means of infrared spectra. Nearly every one of the gasoline components has some characteristic line or lines not shown by any other component. The spectra of benzene, cyclohexane and cyclohexene, for ex-

---

of the hydrocarbons as known up to the end of 1929. The most important work there cited on the present problem is that of Coblentz. J. W. Ellis also, Phys. Rev. **27**, 298 (1926), discusses the work of Coblentz and adds much to the known spectra of liquid materials, including benzene, toluene and certain chain compounds in the region up to 2.8μ, which is accessible with a quartz spectrograph, but he gives no new material for gases, nor for the longer waves. Higher resolution has been applied to certain substances in limited regions of the spectrum by Ellis, by Meyer, Bronk and Levin, by Brackett, and by Bell. Work published since 1929 includes the following:

R. B. Barnes. *Infrared Absorption of Some Organic Liquids under High Resolution.* Phys. Rev. **36**, 296 (1930). Water, benzene and toluene are studied in the region 3 to 4μ. Also in Phys. Rev. **35**, 1524 (1930), Barnes describes work on benzene and eight other cyclic compounds in liquid form in the region 3 to 3.6μ.

J. W. Ellis, Faraday Society Transactions **25**, 611 (1929). These are reports at the symposium on molecular spectra and molecular structure held by the Faraday Society. The work of Ellis (page 888) concerns liquids and the spectral region between 1 and 3μ.

Included in the extensive literature of the Raman spectrum are recent articles of interest in connection with the molecules here studied. It is sufficient to cite two:

P. Krishnamurti, *Complete Raman Spectrum in Relation to Infrared Absorption. Part II. Benzene, Cyclohexane and Octane.* Indian J. Phys. **VI**, 543 (1932).

E. Canals, M. Godchot and G. Canquil. *Raman Spectrum of Some Cyclic Hydrocarbons.* Comptes Rendus **194**, 1374 (1932).

Not a great deal of work bearing directly on the present problem has appeared from the time that the observations given in this paper were completed (in October, 1931) until the date of this writing (July, 1932). However, a paper by P. Lambert and J. Lecomte, Comptes Rendus **194**, 960 (March 14, 1932), gives the location of bands of cyclohexane and cyclohexene and certain heavier compounds. These bands check in wave-length with those of cyclohexane and cyclohexene given here. No curves are shown, however, nor is any indication given of the shape or nature of the bands.

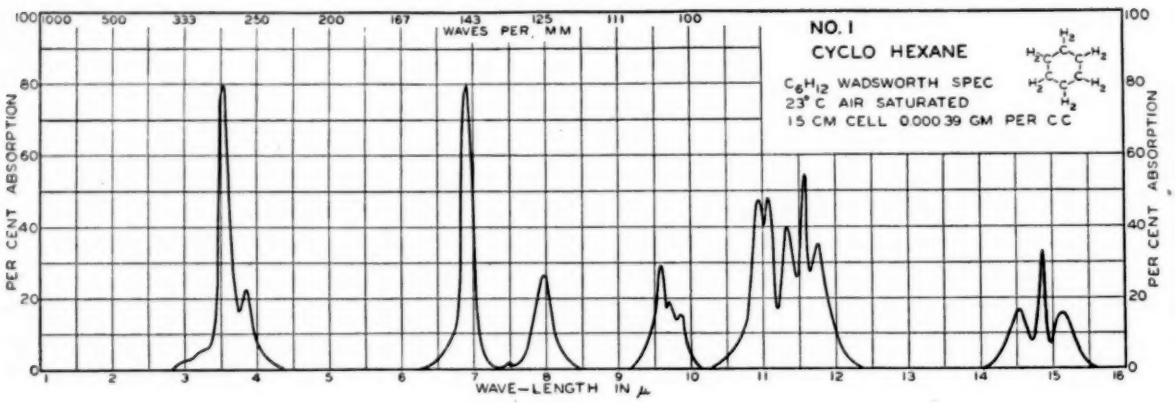
NO. 1
CYCLO HEXANE
C_6H_{12} WADSWORTH SPEC
23° C AIR SATURATED
15 CM CELL 0.00039 GM PER CC
WAVES PER MM
WAVE-LENGTH IN μ
PER CENT ABSORPTION

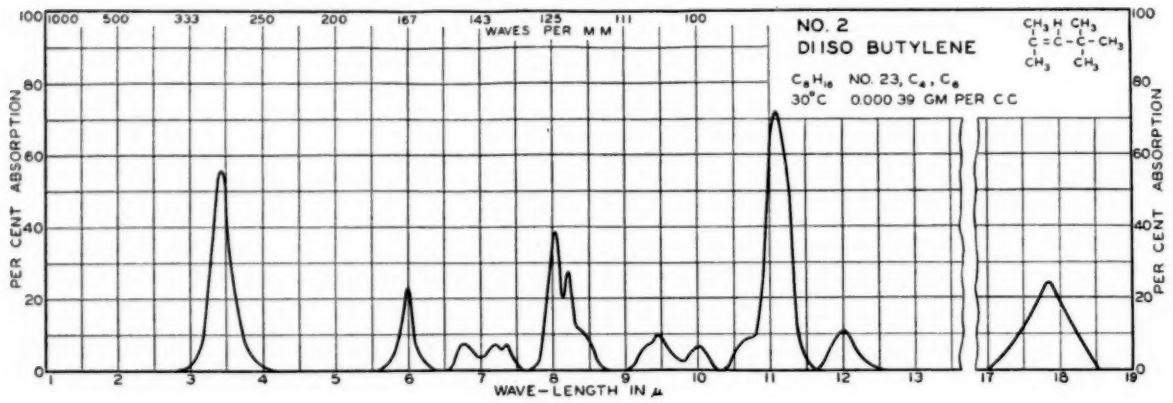
NO. 2
DIISO BUTYLENE
C_8H_{16} NO. 23, C_4, C_8
30°C 0.00039 GM PER CC
WAVES PER MM
WAVE-LENGTH IN μ
PER CENT ABSORPTION

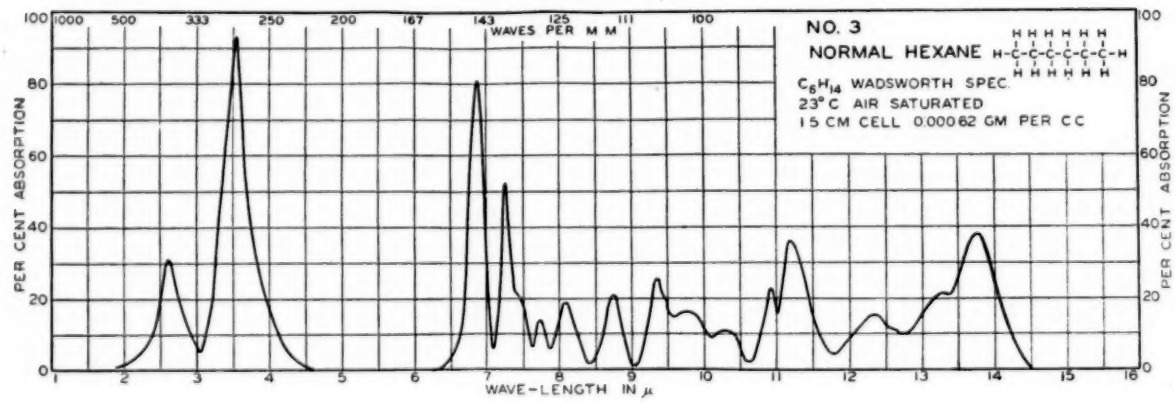
NO. 3
NORMAL HEXANE
C_6H_{14} WADSWORTH SPEC.
23° C AIR SATURATED
15 CM CELL 0.00062 GM PER CC
WAVES PER MM
WAVE-LENGTH IN μ
PER CENT ABSORPTION

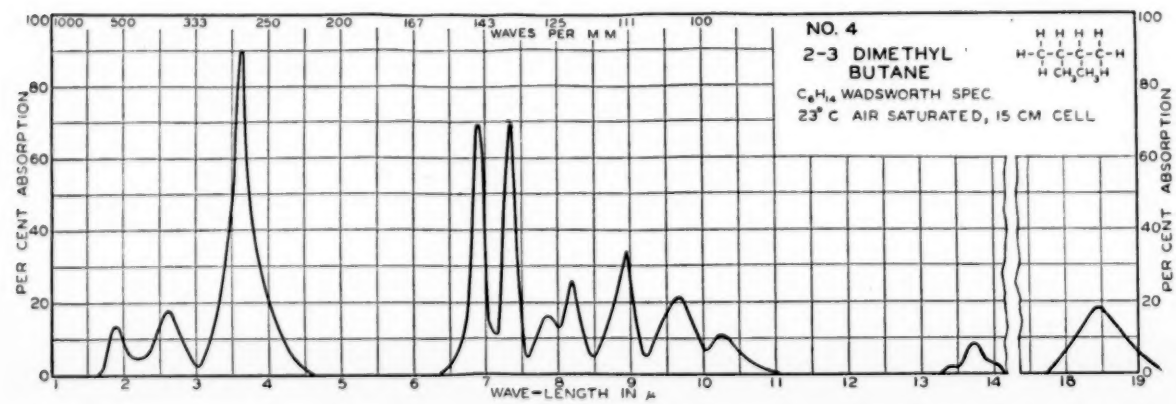
NO. 4
2-3 DIMETHYL BUTANE
C_6H_{14} WADSWORTH SPEC.
23° C AIR SATURATED, 15 CM CELL
WAVES PER MM
WAVE-LENGTH IN μ
PER CENT ABSORPTION

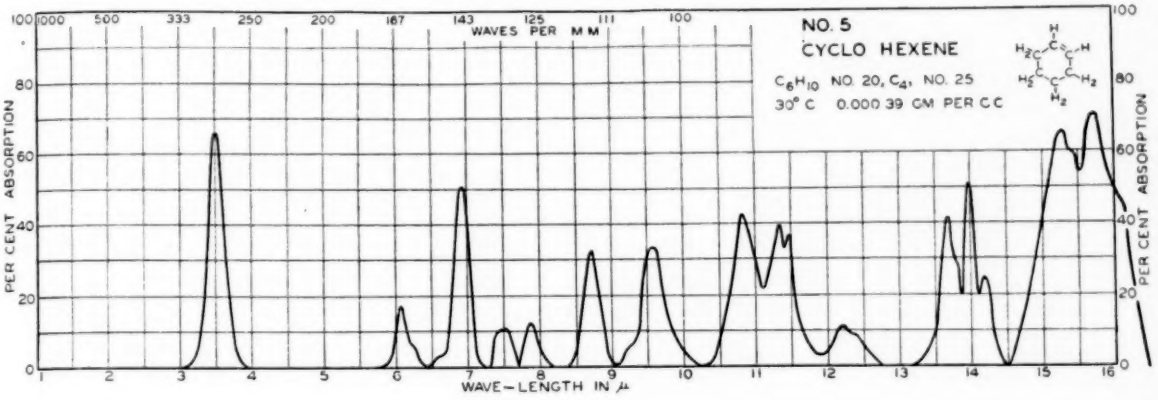
NO. 5
CYCLO HEXENE
C_6H_{10} NO. 20, C_4, NO. 25
30° C 0.000 39 GM PER C C
WAVES PER M M
1000 500 333 250 200 167 143 125 111 100
PER CENT ABSORPTION
WAVE-LENGTH IN μ

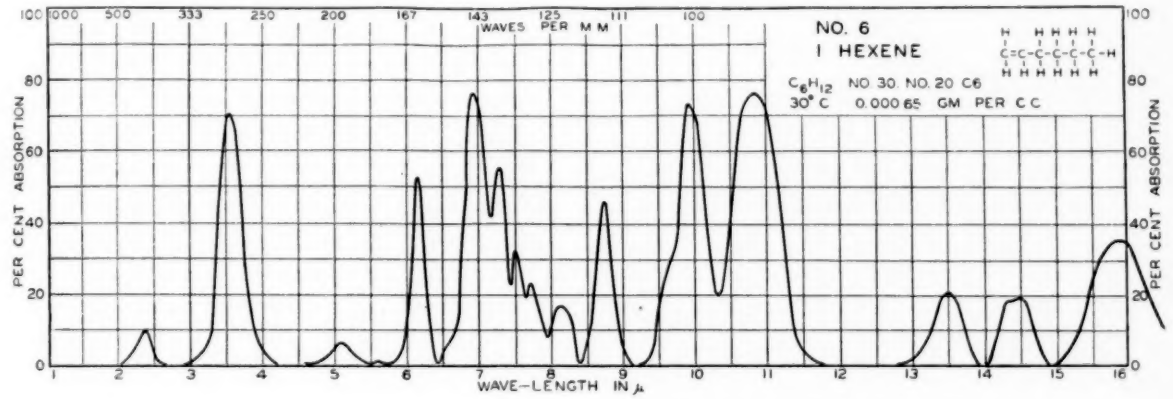
NO. 6
I HEXENE
C_6H_{12} NO. 30. NO. 20 C6
30° C 0.000 65 GM PER C C
WAVES PER M M
1000 500 333 250 200 167 143 125 111 100
PER CENT ABSORPTION
WAVE-LENGTH IN μ

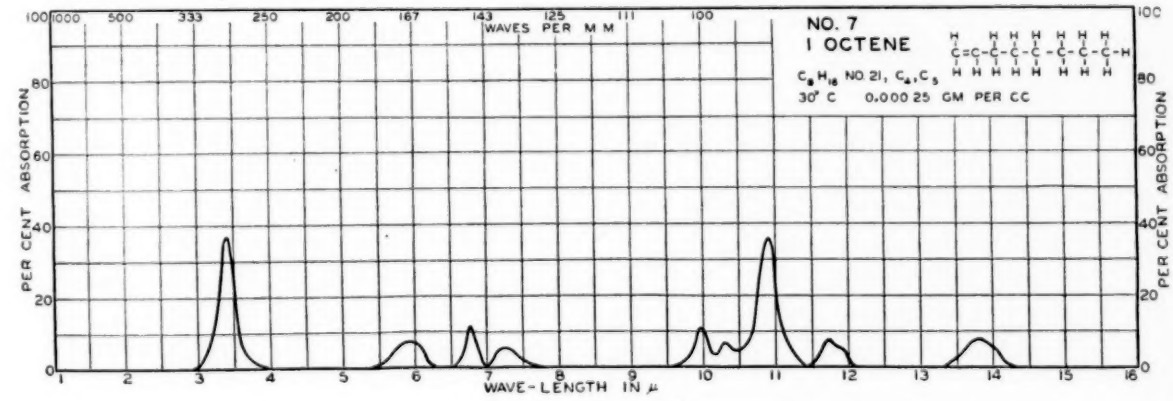
NO. 7
I OCTENE
C_8H_{16} NO 21, C_4, C_5
30° C 0.000 25 GM PER CC
WAVES PER M M
1000 500 333 250 200 167 143 125 111 100
PER CENT ABSORPTION
WAVE-LENGTH IN μ

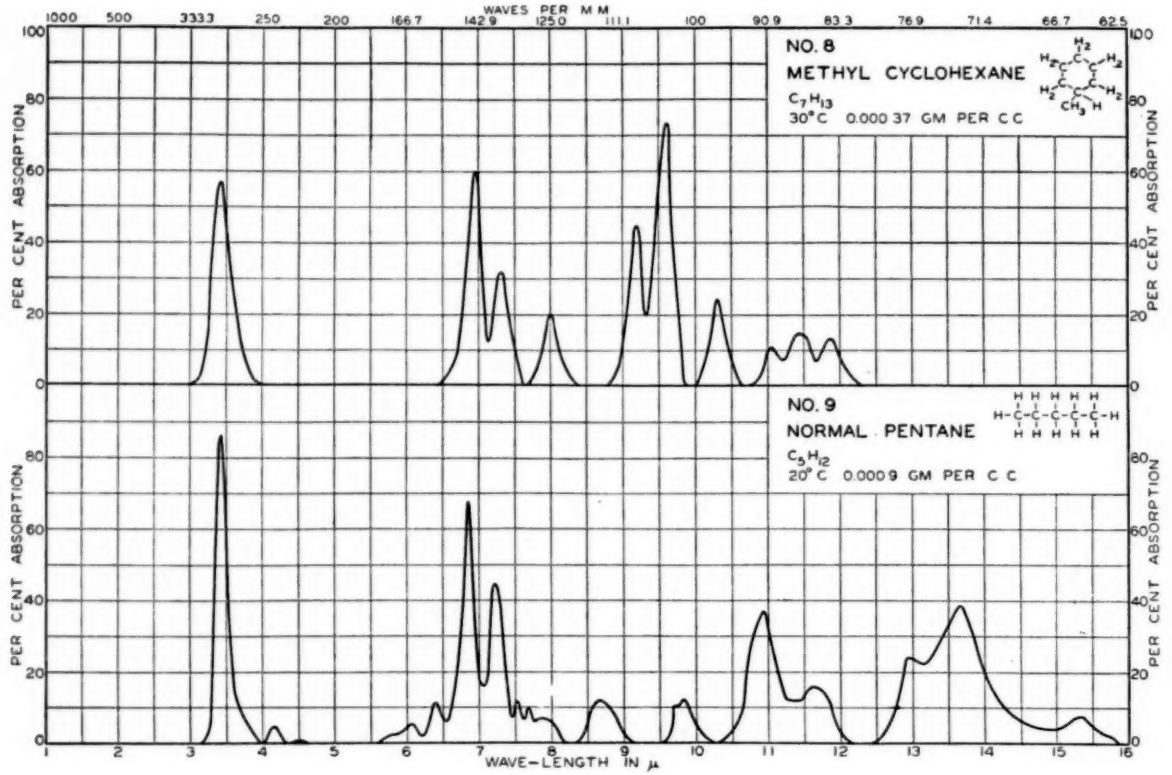
WAVES PER M M
1000 500 333.3 250 200 166.7 142.9 125 111.1 100 90.9 83.3 76.9 71.4 66.7 62.5
NO. 8
METHYL CYCLOHEXANE
C_7H_{13}
30° C 0.000 37 GM PER C C
NO. 9
NORMAL PENTANE
C_5H_{12}
20° C 0.000 9 GM PER C C
PER CENT ABSORPTION
WAVE-LENGTH IN μ

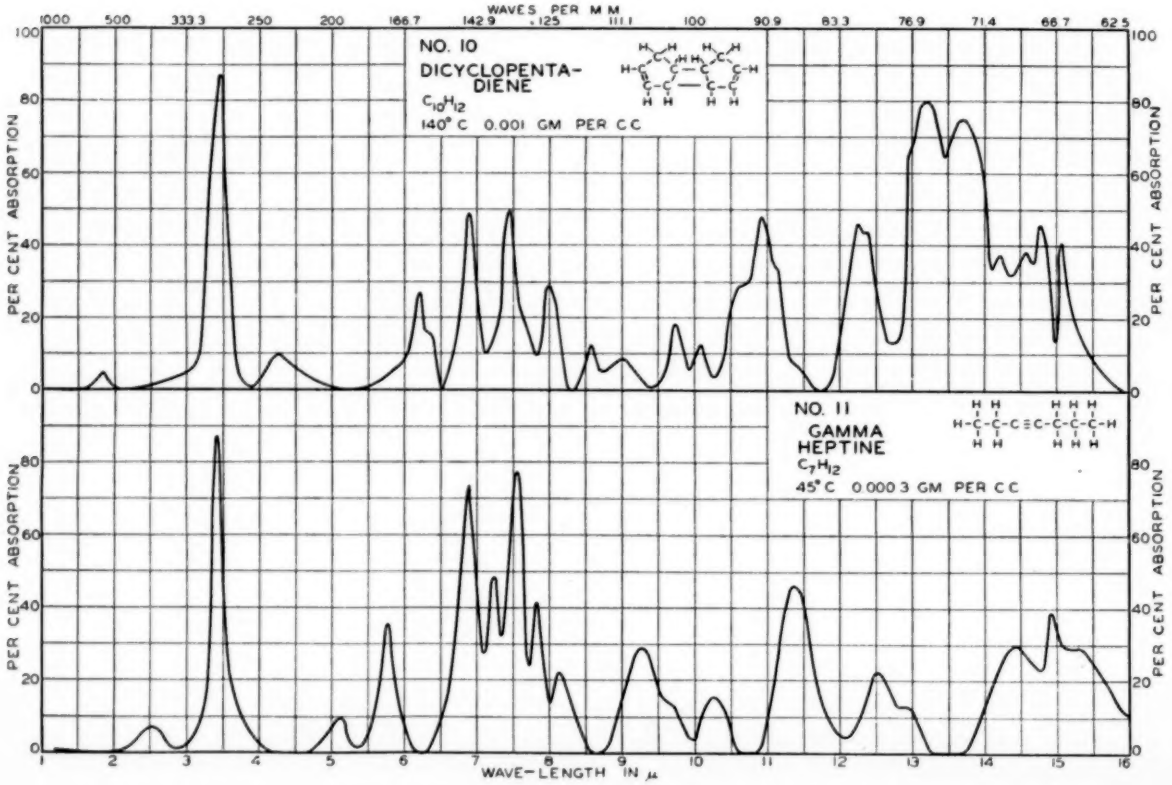
WAVES PER M M
1000 500 333.3 250 200 166.7 142.9 125 111.1 100 90.9 83.3 76.9 71.4 66.7 62.5
NO. 10
DICYCLOPENTA-DIENE
$C_{10}H_{12}$
140° C 0.001 GM PER C C
NO. 11
GAMMA HEPTINE
C_7H_{12}
45° C 0.000 3 GM PER C C
PER CENT ABSORPTION
WAVE-LENGTH IN μ

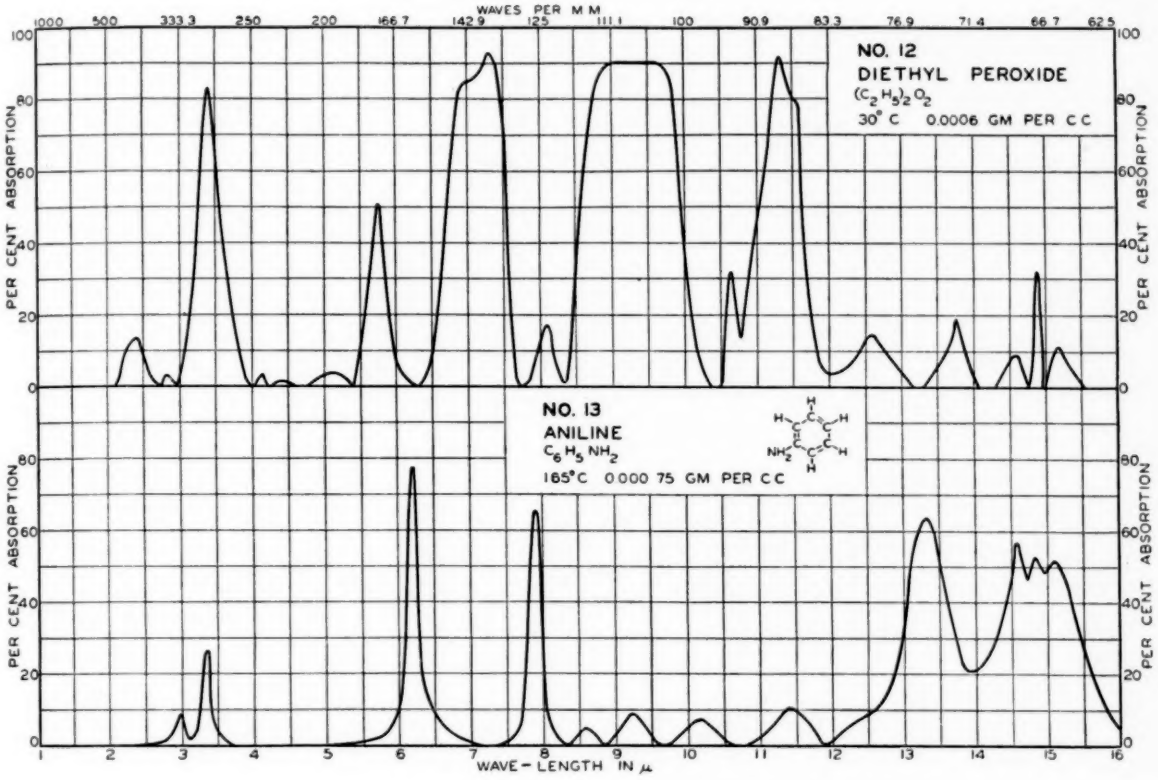
WAVES PER M M
1000 500 333.3 250 200 166.7 142.9 125 111.1 100 90.9 83.3 76.9 71.4 66.7 62.5
PER CENT ABSORPTION
NO. 12
DIETHYL PEROXIDE
$(C_2H_5)_2O_2$
30° C 0.0006 GM PER C C
NO. 13
ANILINE
$C_6H_5NH_2$
165°C 0.000 75 GM PER C C
WAVE-LENGTH IN μ

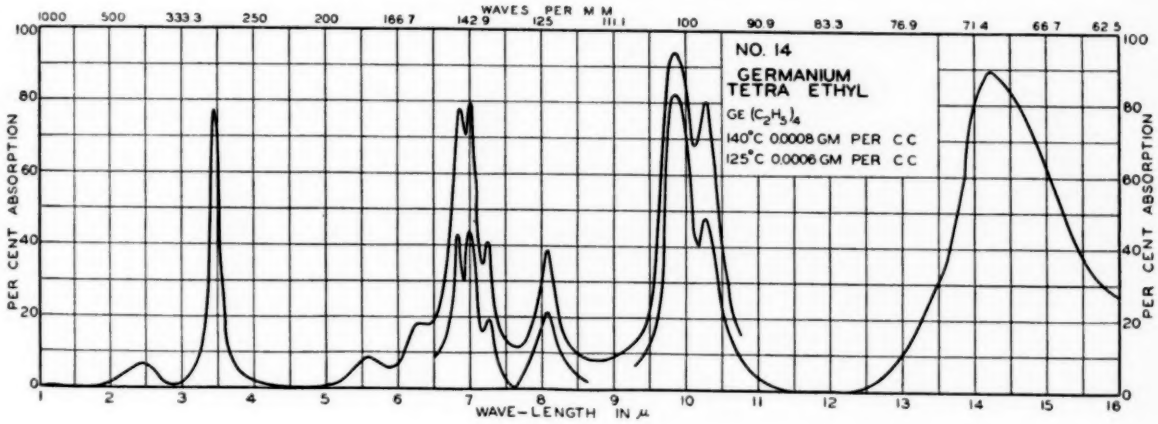
WAVES PER M M
1000 500 333.3 250 200 166.7 142.9 125 111.1 100 90.9 83.3 76.9 71.4 66.7 62.5
PER CENT ABSORPTION
NO. 14
GERMANIUM
TETRA ETHYL
GE $(C_2H_5)_4$
140°C 0.0008 GM PER C C
125°C 0.0006 GM PER C C
WAVE-LENGTH IN μ

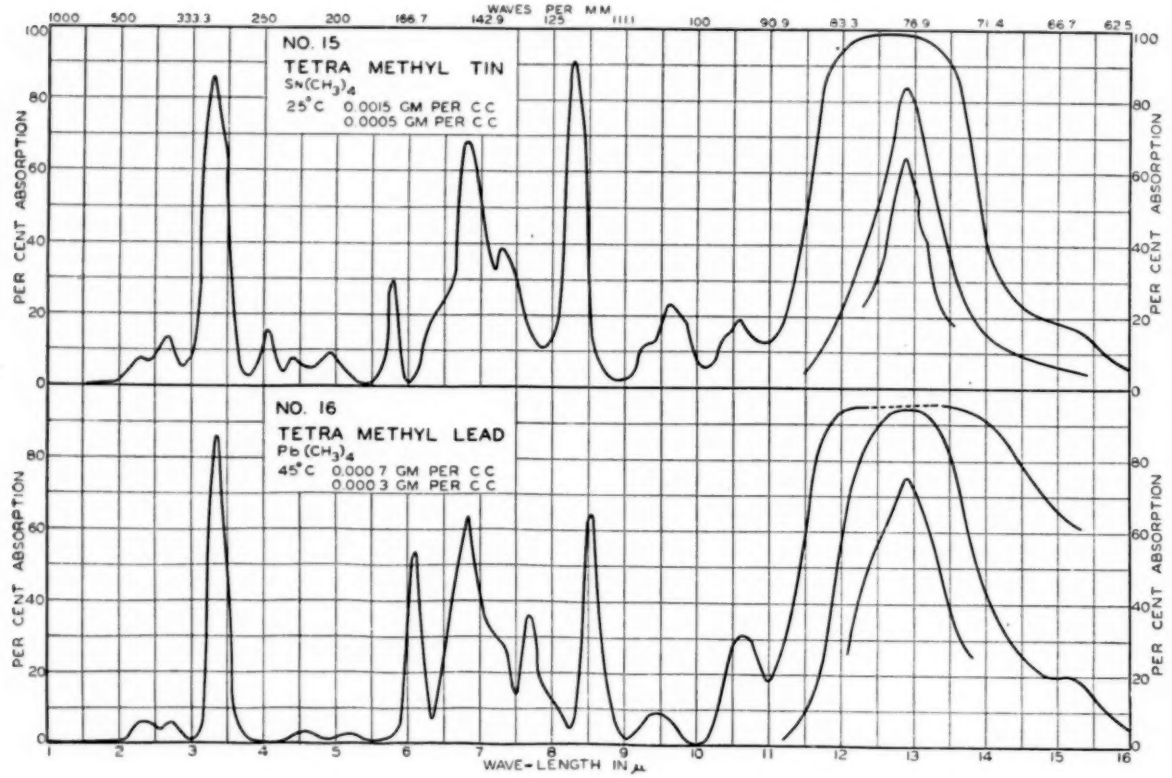
WAVES PER MM
1000 500 333.3 250 200 166.7 142.9 125 111 100 90.9 83.3 76.9 71.4 66.7 62.5
NO. 15
TETRA METHYL TIN
$Sn(CH_3)_4$
25°C 0.0015 GM PER C C
0.0005 GM PER C C
NO. 16
TETRA METHYL LEAD
$Pb(CH_3)_4$
45°C 0.0007 GM PER C C
0.0003 GM PER C C
PER CENT ABSORPTION
WAVE-LENGTH IN μ

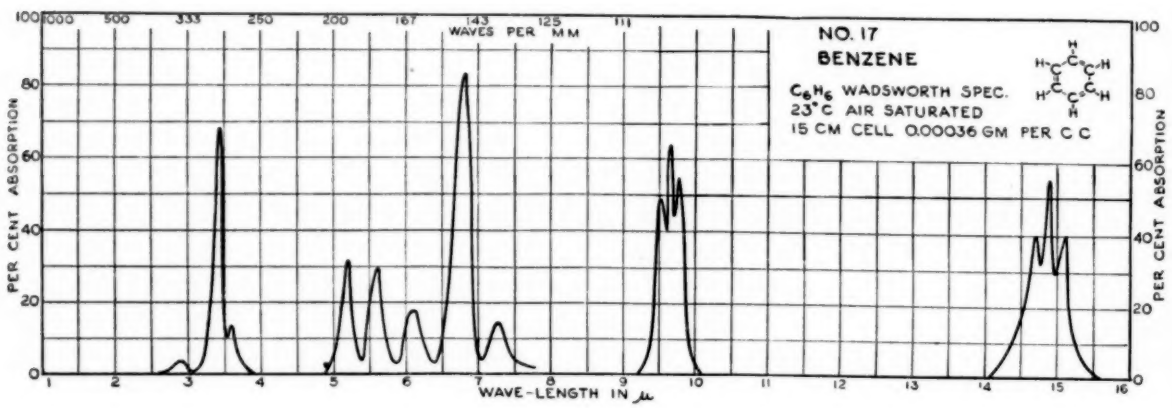
WAVES PER MM
1000 500 333 250 200 167 143 125 111
NO. 17
BENZENE
C_6H_6 WADSWORTH SPEC.
23°C AIR SATURATED
15 CM CELL 0.00036 GM PER C C
PER CENT ABSORPTION
WAVE-LENGTH IN μ

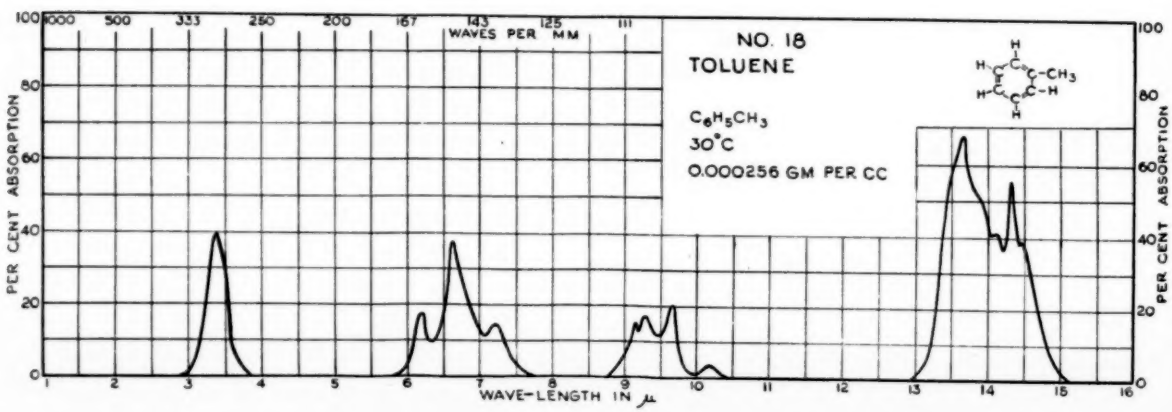
WAVES PER MM
1000 500 333 250 200 167 143 125 111
NO. 18
TOLUENE
$C_6H_5CH_3$
30°C
0.000256 GM PER CC
PER CENT ABSORPTION
WAVE-LENGTH IN μ

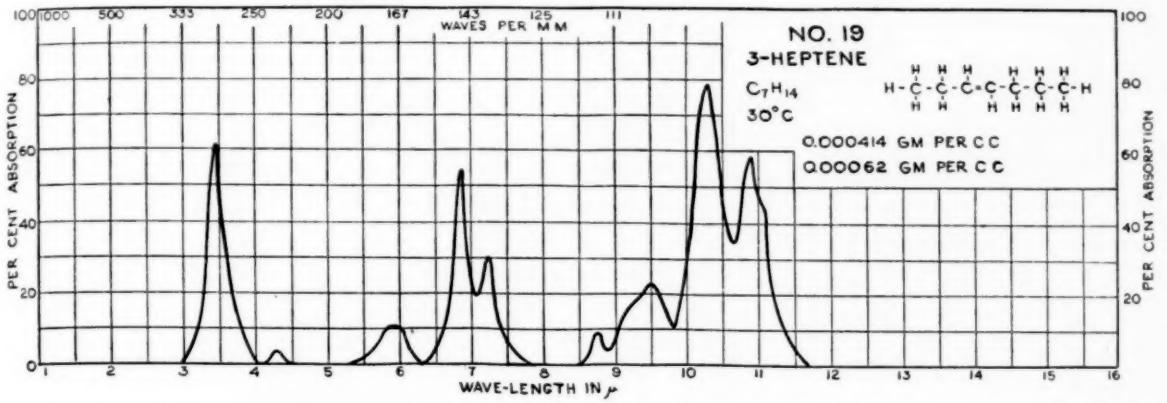
NO. 19
3-HEPTENE
C_7H_{14}
30°C
0.000414 GM PER C C
0.00062 GM PER C C
WAVES PER M M
PER CENT ABSORPTION
WAVE-LENGTH IN μ

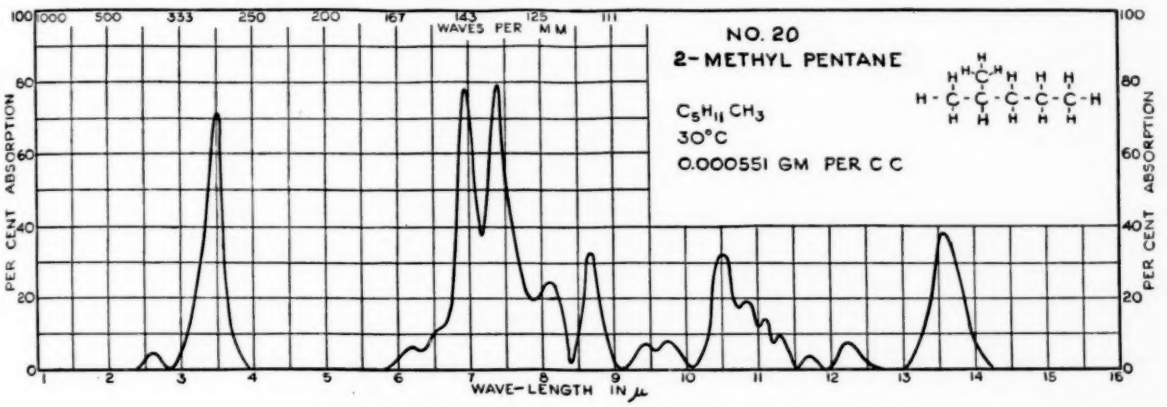
NO. 20
2-METHYL PENTANE
$C_5H_{11}CH_3$
30°C
0.000551 GM PER C C
WAVES PER M M
PER CENT ABSORPTION
WAVE-LENGTH IN μ

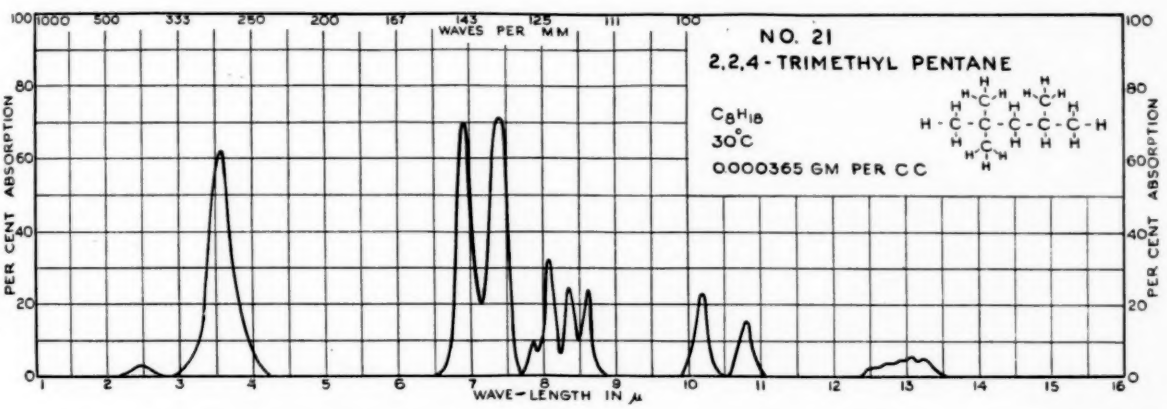
NO. 21
2,2,4-TRIMETHYL PENTANE
C_8H_{18}
30°C
0.000365 GM PER C C
WAVES PER M M
PER CENT ABSORPTION
WAVE-LENGTH IN μ

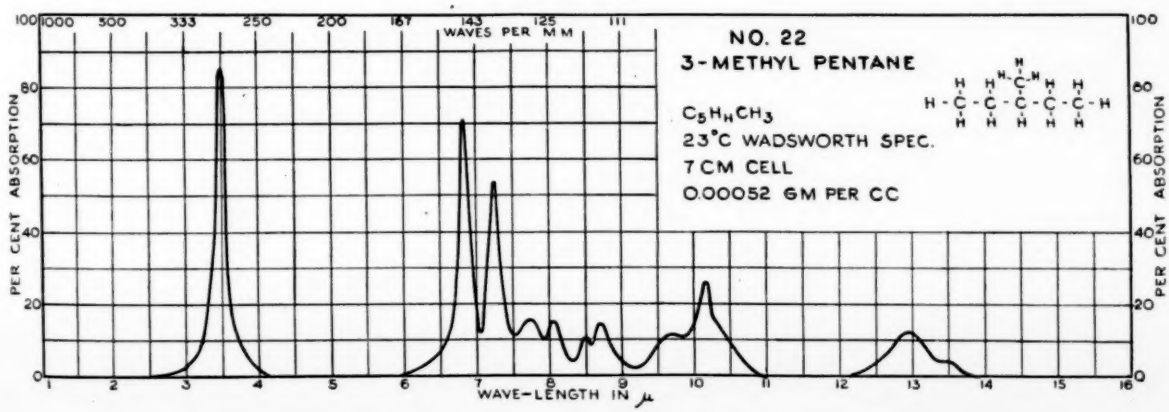
NO. 22
3-METHYL PENTANE
$C_5H_HCH_3$
23°C WADSWORTH SPEC.
7 CM CELL
0.00052 GM PER CC
WAVES PER M M
PER CENT ABSORPTION
WAVE-LENGTH IN μ

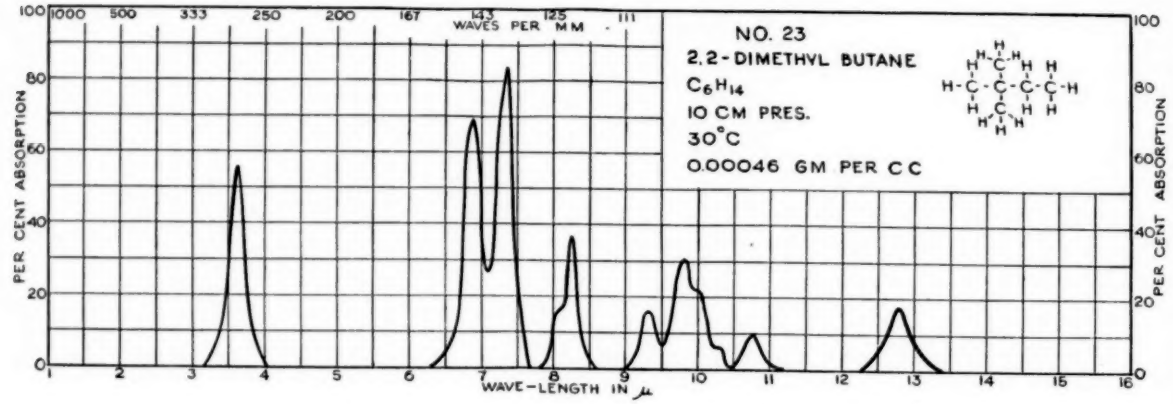
NO. 23
2.2-DIMETHYL BUTANE
C_6H_{14}
10 CM PRES.
30°C
0.00046 GM PER CC
WAVES PER MM
PER CENT ABSORPTION
WAVE-LENGTH IN μ

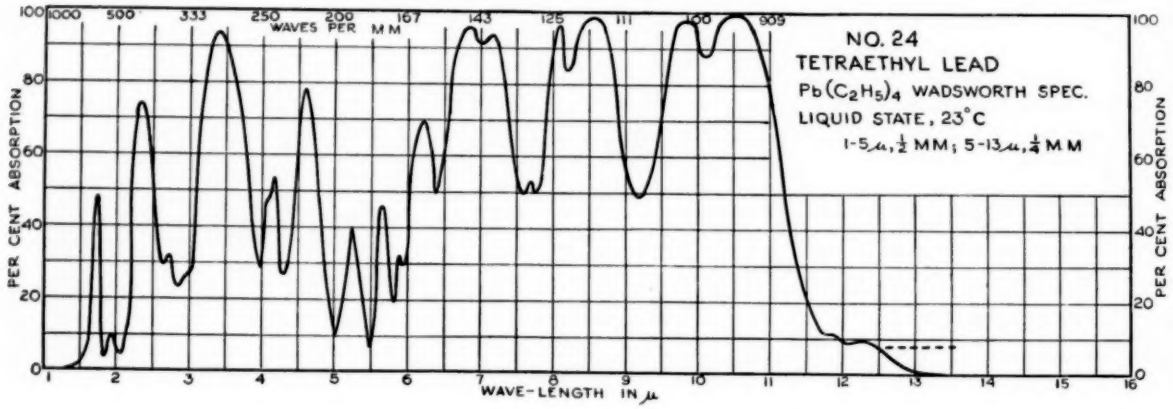
NO. 24
TETRAETHYL LEAD
$Pb(C_2H_5)_4$ WADSWORTH SPEC.
LIQUID STATE, 23°C
1-5μ, ½ MM; 5-13μ, ¼ MM
WAVES PER MM
PER CENT ABSORPTION
WAVE-LENGTH IN μ

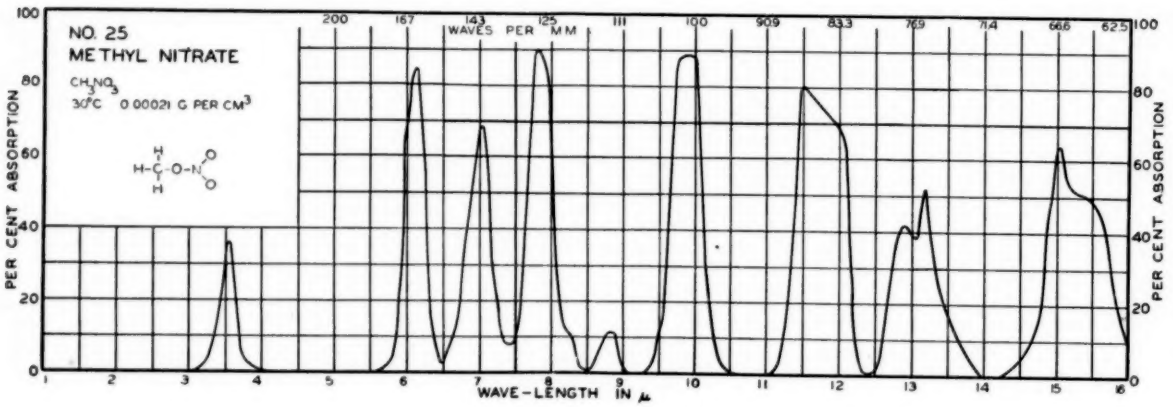
NO. 25
METHYL NITRATE
CH_3NO_3
30°C 0.00021 G PER CM^3
WAVES PER MM
PER CENT ABSORPTION
WAVE-LENGTH IN μ

ample, though similar in certain respects, show unmistakable differences. That of cyclohexene has unsymmetrical bands, the location of which could hardly be predicted from the wave-lengths shown by the absorption of benzene and cyclohexane. In this connection something may be said about the sources and the purity of the materials employed. All the samples were sent to the university from the Research Laboratory of the General Motors Corporation at Detroit. Mr. Paul M. Cramer of that laboratory has prepared the following statement about the materials:

> With the exception of nickel carbonyl, germanium tetraethyl, tetramethyl tin and methyl nitrate, all the compounds included in this work were either prepared or repurified in this laboratory. Many of the compounds were obtained from outside sources. In only one or two cases is there any reasonable doubt about the purity of the compounds. The boiling-point range of the compounds was within narrow limits, 0.5°C or less, and the physical constants were in close agreement with the accepted values given in the literature.
>
> *n*-Hexane, benzene, cyclohexene, cyclohexane, toluene, methyl cyclohexane, *n*-pentane, nickel carbonyl, methyl nitrate and methyl iodide were obtained from the Eastman Kodak Company.
>
> Diiso butylene and 2, 2, 4-trimethyl pentane were obtained from the Ethyl Gasoline Corporation. The sample of diiso butylene consisted of a mixture of two isomers, 2, 2, 4-trimethyl pentene-4 and 2, 2, 4-trimethyl pentene-3.
>
> Dicylcopentadiene, a coal-tar product obtained from the Gesellschaft für Teerverwertung, was carefully fractionated under reduced pressure. Since the reaction of cyclopentadiene to dicyclopentadiene is reversible at 170°C, there are probably traces of cyclopentadiene and also higher polymers at room temperature.
>
> The aniline was purified by the recrystallization of the hydrochloride prepared from aniline obtained from the Dow Chemical Company.
>
> The sample of tetraethyl germanium was furnished by L. M. Dennis of Cornell University.
>
> The tetramethyl tin was obtained from C. A. Kraus of Brown University.

The work at the university was done with the assistance of Mr. P. E. Martin, Mr. John Strong and Mr. V. H. Fraenckel. It has profited by the cooperation of many members of the staff of the Physics Department, and in particular by the help of Professor Barker and Professor Randall.

Some points of interest appear in connection with the spectra of the compounds containing the tetra-valent metals, tin, lead and germanium. They show no double or triple bands, such as appear in the spectra of benzene and cyclohexane, but they have, like the hydrocarbons, strong bands at about 3.4μ and in the neighborhood of 7μ. These materials require the use of the heated cell, and these are the only spectra not carried beyond the range of the Wadsworth spectrometer, that is beyond 16μ.

General Properties of Steady Temperatures in Solids Partially Exposed to Gas

R. V. CHURCHILL, *Department of Mathematics, University of Michigan*

(Received January 3, 1933)

Five general properties of steady temperatures in solids of arbitrary shape are derived here. Although the derivations are mathematical they depend almost solely on the very fundamentals of the mathematical theory of heat conduction. The solid has any portion of its surface held at a fixed temperature distribution and the rest exposed to gas. The rate of transfer of heat between gas and surface is assumed to be any function of the position of the point and the temperature of the surface, for a given state of the gas. For a fixed temperature this function is called the emissivity. Briefly stated, the important properties are: I. In two geometrically similar solids exposed to the same surface temperature conditions at corresponding points, except that their emissivities are inversely proportional to their sizes, the temperatures at corresponding points are equal. I(a). If the entire surfaces of two geometrically similar solids are given fixed temperature distributions the temperatures at corresponding points are equal everywhere if they are equal on the surfaces. II. An increase in the size of a solid causes the same temperature change as an increase in its emissivity. IV. An increase in the size of a solid causes an increase in the temperature at each point if the solid is receiving heat from the gas, and a decrease if the solid is losing heat to the gas. V. From Newton's law of surface heat transfer there follows a linear relation between the steady temperature at any point and the uniform temperatures of the gas and the fixed-temperature surface. These properties are discussed at the end of the paper. Some of the results of IV seem contrary to expected results.

IN a mathematical study of the thermal design of spark plug insulators[1] the author found several properties of temperatures in solids partially exposed to gas which could be generalized so as to be applicable to a variety of problems in physics and engineering. These generalized properties, which are believed to be new, are derived here from the fundamentals of the mathematical theory of heat conduction. They are of special importance in problems in which solids of the same shape but constructed to different scales are subjected to similar temperature conditions (see Properties IV and I(a)).

Except in Property V, the law assumed for the transfer of heat between the gas and the solid is very general, so it seems that few restrictions on the usefulness of the properties should be experienced on its account.

All temperatures considered here are those which exist after a steady state of temperatures is reached. The solids are assumed to be homogeneous and isotropic, and to have constant thermal conductivities. Their shapes are arbitrary.

The properties derived here apply to a solid exposed to a gas over any regions of its surface. To the remainder of the surface any definite temperature distribution is assigned. These two portions of the boundary of the solid are referred to hereafter as the exposed surface, $g(x, y, z)=0$, and the fixed-temperature surface $f(x, y, z)=0$.

At the exposed surface, for any given state of the gas, a general relation is assumed between the coordinates of the point, the temperature T, and the temperature gradient normal to the surface at the point:

$$dT/dn=\phi(x, y, z, T) \quad \text{on} \quad g(x, y, z)=0, \quad (1)$$

where n is the outward drawn normal to the surface.

In the first four properties this general law (1) is restricted only to this extent: It is assumed that the function $\phi(x, y, z, T)$ cannot increase with T at any point. This is a natural restriction since it implies that the absolute value of the temperature gradient normal to the surface, or of the rate of transfer of heat across the surface, cannot increase when the surface temperature approaches the gas temperature. In Property V

[1] This work was done for the Department of Engineering Research, University of Michigan. To the AC Spark Plug Company of Flint, Michigan, which company suggested and supported this work, the author makes grateful acknowledgment.

a very special case of Eq. (1), known as Newton's law of surface heat transfer, is used; and in Property I(a) no gas is involved.

The rate of transfer of heat across the exposed surface depends upon the value of the function ϕ. For a fixed T we shall refer to this function as the emissivity function. Then by an increase in this function, or an increase in emissivity, we shall mean a change to a new function ϕ' which is greater than ϕ at each point of the exposed surface, for the same T; that is, $\phi'(x, y, z, T) > \phi(x, y, z, T)$ for all T, x, y, z.

Property I

Consider any two geometrically similar solids with corresponding portions of their boundary surfaces held at fixed temperatures and the remaining portions exposed to gas. If the temperatures are the same at corresponding points of the fixed-temperature surfaces and if the emissivities at corresponding points of the exposed surfaces are inversely proportional to the sizes of the solids, then the temperatures at corresponding points throughout the two solids are equal.

To prove this property we must first make clear the meaning of similarity. Two solids are geometrically similar if their boundary surfaces can be placed relative to each other so that they are in perspective with respect to some point O. That is, if P is any point on one surface then there is a point P' on the other so that the vectors (OP') and (OP) satisfy the condition $(OP') = \alpha(OP)$, where α is the same for all points P.

Then if O is taken as the origin a point (x, y, z) on the first surface has $(\alpha x, \alpha y, \alpha z)$ for its corresponding point on the second; distances between corresponding pairs of points have the ratio $1/\alpha$, while the directions of the lines joining these pairs are the same. It also follows that if $S(x, y, z) = 0$ is the equation of the boundary surface of the first solid then $S(x/\alpha, y/\alpha, z/\alpha) = 0$ is the equation of that of the second, and the normals to these two surfaces at corresponding points are parallel.

The differential equation and boundary conditions which determine the temperature in the first solid are

$$\partial^2 T/\partial x^2 + \partial^2 T/\partial y^2 + \partial^2 T/\partial z^2 = 0 \quad \text{throughout the solid,} \quad (2)$$

$$T = T_0(x, y, z) \quad \text{on the surface } f(x, y, z) = 0, \quad (3)$$

$$dT/dn = \phi(x, y, z, T) \quad \text{on the surface } g(x, y, z) = 0, \quad (1)$$

where $T_0(x, y, z)$ is any function of x, y and z. Let $T = F(x, y, z)$ be the temperature distribution determined by these conditions.

Let us substitute the new independent variables $x' = \alpha x$, $y' = \alpha y$, $z' = \alpha z$ throughout this problem, where α is a constant. The solution becomes $T = F(x'/\alpha, y'/\alpha, z'/\alpha)$. If λ, μ, ν are the direction cosines of the normal to the surface $g(x, y, z) = 0$ at (x, y, z), then

$$\frac{dT}{dn} = \frac{\partial T}{\partial x}\lambda + \frac{\partial T}{\partial y}\mu + \frac{\partial T}{\partial z}\nu = \alpha\left(\frac{\partial T}{\partial x'}\lambda + \frac{\partial T}{\partial y'}\mu + \frac{\partial T}{\partial z'}\nu\right).$$

Since the direction cosines of the normal to $g(x, y, z) = 0$ at (x, y, z) are the same as those of the normal to $g(x'/\alpha, y'/\alpha, z'/\alpha) = 0$ at (x', y', z') the expression in parentheses in the last equation becomes dT/dn', when n' is the normal to $g(x'/\alpha, y'/\alpha, z'/\alpha) = 0$.

In terms of the new variables then, Eqs. (2), (3), and (1) become

$$\partial^2 T/\partial x'^2 + \partial^2 T/\partial y'^2 + \partial^2 T/\partial z'^2 = 0 \quad \text{for all } x', y', z', \quad (2')$$

$$T = T_0(x'/\alpha, y'/\alpha, z'/\alpha) \quad \text{when } f(x'/\alpha, y'/\alpha, z'/\alpha) = 0, \quad (3')$$

$$dT/dn' = \alpha^{-1}\phi(x'/\alpha, y'/\alpha, z'/\alpha, T) \quad \text{when } g(x'/\alpha, y'/\alpha, z'/\alpha) = 0. \quad (1')$$

When we interpret x', y', z' as the coordinates of a point, the surfaces $f(x'/\alpha, y'/\alpha, z'/\alpha) = 0$ and $g(x'/\alpha, y'/\alpha, z'/\alpha) = 0$ are in perspective with the surfaces $f(x, y, z) = 0$ and $g(x, y, z) = 0$. Hence Eqs. (1'), (2'), (3') are the complete set of conditions for the problem of temperature distribution in a solid geometrically similar to the first and α times as large.

According to Eq. (3') the temperature at (x', y', z') on the fixed-temperature surface is the same as that at the corresponding point of the first solid. Eq. (1') shows that for equal

temperatures at corresponding points of the exposed surfaces of the two solids the normal gradient of T at the exposed surface of the second is $1/\alpha$ times its value at the corresponding point of the first; that is, the emissivity of the second is $1/\alpha$ times that of the first.

Since the function $T=F(x'/\alpha, y'/\alpha, z'/\alpha)$ satisfies the conditions (1′), (2′), (3′), it gives the temperature distribution in the second solid. It shows that the temperature at (x', y', z') is the same as that at the corresponding point $(x'/\alpha, y'/\alpha, z'/\alpha)$ in the first solid. Hence Property I is proved.

Property II

An increase in the size of a solid causes the same temperature change as a proportionate increase in its emissivity.

More precisely, consider a given solid and a second one geometrically similar to it but α times as large. Let these solids have equal temperatures at corresponding points of their fixed-temperature surfaces, and equal values for their emissivity functions at corresponding points of their exposed surfaces, that is, $\phi'(x', y', z', T) = \phi(x, y, z, T)$. Then the temperature at each point of a third solid, identical to the first except that its emissivity function is α times as large, will be the same as the temperature at the corresponding point of the second.

This is a corollary of Property I. Let $\phi(x, y, z, T)$ be the emissivity function at (x, y, z) of the first solid. Then at (x', y', z') of the second, where $x'=\alpha x$, $y'=\alpha y$, $z'=\alpha z$, the emissivity function is $\phi(x'/\alpha, y'/\alpha, z'/\alpha, T)$, and at (x, y, z) of the third it is $\alpha\phi(x, y, z, T)$. The emissivities of the second and third are therefore inversely proportional to their sizes so the temperatures at corresponding points are equal, according to Property I.

In the next two properties the assumption will be made that the temperature determined by our conditions (1), (2), (3) is continuous over the surface of the solid as well as throughout its interior.

Property III

Except at points on the fixed-temperature surface, the temperature at each point of a solid increases as a result of an increase in the value of its emissivity function at all points of the exposed surface.

Let us state this property for each of the two cases $\phi>0$ and $\phi<0$. In a solid which receives heat from a gas at all points of its exposed surface the temperature at any point cannot decrease when the value of the emissivity function is increased. But in a solid which loses heat to a gas at all points of its exposed surface the temperature at any point cannot increase when the absolute value of the emissivity function increases. It is only on the fixed-temperature surface that the temperature remains unchanged.

This property may seem too obvious physically to deserve a mathematical proof; but it leads directly to Property IV which, in some of its applications, seems to defy intuition.

In a solid with emissivity function ϕ the temperature T satisfies Eqs. (1), (2), (3). Let T' be the temperature in a solid of the same size and shape subject to the same surface temperature conditions except that its emissivity function is increased:

$$\phi'(x, y, z, T') > \phi(x, y, z, T') \text{ on } g(x, y, z)=0. \quad (4)$$

This increase may be due, for example, to a change in the state of the gas.

Then T' satisfies the conditions

$$\partial^2T'/\partial x^2+\partial^2T'/\partial y^2+\partial^2T'/\partial z^2=0$$

throughout the solid,

$$T'=T_0(x, y, z) \quad \text{on} \quad f(x, y, z)=0,$$

$$dT'/dn=\phi'(x, y, z, T') \quad \text{on} \quad g(x, y, z)=0.$$

Now let $u=T'-T$; then according to the above conditions on T and T', u must satisfy the equations

$$\partial^2u/\partial x^2+\partial^2u/\partial y^2+\partial^2u/\partial z^2=0$$

throughout the solid, (5)

$$u=0 \quad \text{on} \quad f(x, y, z)=0, \quad (6)$$

$$du/dn=\phi'(x, y, z, T')-\phi(x, y, z, T)$$

on $g(x, y, z)=0$. (7)

Suppose that the function u which satisfies these three conditions has at some point P a minimum value which is negative. Then the

point P must lie on the surface $g(x, y, z)=0$. For u is a harmonic function, according to Eq. (5), and the minimum value of such a function is assumed only on the boundary of the solid,[2] unless u is the same at all points. However, u is not negative on $f(x, y, z)=0$ because of Eq. (6).

Hence at some point P of $g(x, y, z)=0$ we should have $T>T'$ and, since ϕ does not increase with T, it would follow that

$$\phi(x, y, z, T') \geqq \phi(x, y, z, T).$$

Condition (4) then gives the inequality

$$\phi'(x, y, z, T') > \phi(x, y, z, T') \geqq \phi(x, y, z, T) \text{ at } P,$$

and according to Eq. (7), this means that du/dn is positive at P. But this implies that u increases toward its minimum value at P, which is obviously a contradiction. The minimum value of u is therefore zero.

Now u cannot be the same at all points since this would mean $u=0$, and $T=T'$, everywhere, whereas the conditions (4) and (7) require du/dn to be different from zero on $g(x, y, z)=0$. Moreover u cannot assume this minimum value on the exposed surface since the conditions (4) and (7) require du/dn to be positive there. Hence $u=0$ on the fixed-temperature surface only, and $u>0$ elsewhere.

The temperature T' is therefore greater than T at each point not on the fixed-temperature surface, where $T'=T$, and Property III is proved.

Property IV

An increase in the size of a solid to one geometrically similar to the original causes an increase in its temperature if the solid is receiving heat from the gas, and a decrease in its temperature if the solid is losing heat to the gas.

To make this important property clear, consider two solids which are geometrically similar and subject to the same fixed temperatures and equal emissivity functions at corresponding points of their surfaces; that is, $T_0(x, y, z) = T_0'(\alpha x, \alpha y, \alpha z)$ on fixed temperature surfaces, $\phi(x, y, z, T)=\phi'(\alpha x, \alpha y, \alpha z, T)$ on exposed surfaces. Then the temperature at each point of the larger solid is higher than that at the corresponding point of the smaller provided heat is flowing from the gas to the solids. If heat is flowing from the solids to the gas then the temperature at each point of the larger solid is lower than that at the corresponding point of the smaller. At corresponding points of the fixed-temperature surfaces, of course, the temperatures are equal.

This property follows easily from Properties II and III. A solid which is α times as large as the original but subject to the same surface temperature conditions has a temperature at each point equal to that which would occur at the corresponding point of the original if the emissivity of the original were multiplied by α (Property II). Take $\alpha>1$, and suppose that heat flows from gas to solids ($\phi>0$ everywhere). It follows from Property III that the temperature at each point of the large solid, except for the fixed-temperature surface, is higher than that at the corresponding point of the original. Similarly if we suppose that heat flows from the solids to the gas ($\phi<0$ everywhere), it follows from Property III that the temperatures in the large solid are lower than the corresponding temperatures in the original.

Property V

When Newton's law of heat transfer at the exposed surface applies and the temperature T_0 is uniform over the fixed-temperature surface, the steady temperature T at any point of the solid bears a linear relation to the temperature of the gas T_g and the temperature T_0:

$$T = WT_g + (1-W)T_0. \tag{8}$$

The quantity W depends for its value upon the design of the solid, the coordinates of the point at which T is measured, and the thermal coefficient h in Newton's law (10) below.

The temperature T is determined by the three conditions

$$\partial^2 T/\partial x^2 + \partial^2 T/\partial y^2 + \partial^2 T/\partial z^2 = 0 \quad \text{at all points},$$
$$T = T_0 \quad \text{on} \quad f(x, y, z)=0,$$
$$dT/dn = h(T_g - T) \quad \text{on} \quad g(x, y, z)=0, \tag{9}$$

where h is a constant. If we substitute the new variable

[2] See Riemann-Weber's *Differentialgleichungen der Physik* I, 1925, p. 571, or MacMillan, *Theory of the Potential*, 1930, p. 134.

$$W=(T-T_0)/(T_g-T_0) \qquad (10)$$

these three conditions become $\partial^2 W/\partial x^2+\partial^2 W/\partial y^2+\partial^2 W/\partial z^2=0$, $W=0$ on $f(x, y, z)=0$, $dW/dn=h(1-W)$ on $g(x, y, z)=0$.

But these are the complete set of conditions for determining the steady temperature W at any point of the given solid whose surface $f(x, y, z)=0$ is held at zero temperature while the remainder of its boundary $g(x, y, z)=0$ is exposed to Newton's transfer of heat from a gas with unit temperature. Hence W depends upon x, y, z, the value of the constant h, and the design of the solid. Since the linear Eq. (9) is another form of Eq. (11), Property V is proved.

Discussion of Properties

It should be noted that insulated regions of the boundary surface are not excluded in the above properties since $\phi=0$ on the region insulated is the mathematical condition for this case. In such cases a minor change is necessary in Property IV, however. In our proof, extended by assuming a continuously varying T as ϕ approaches zero over any region, we would not exclude the possibility of T being the same at corresponding points on these insulated surfaces of the two solids.

When the two solids of Property I are placed in perspective it is clear that the isothermal surfaces in the two solids for any given temperature are also in perspective. This is true for any two geometrically similar solids with their entire boundary surfaces held at corresponding fixed temperature distributions. To prove this all we need do is to modify the conditions in our proof of Property I as follows. Let $f(x, y, z)=0$ be the entire boundary surface of the first solid, so that $f(x'/\alpha, y'/\alpha, z'/\alpha)=0$ is that of the second, and drop the conditions (1) and (1′), so that the function ϕ is not involved. The following important special case of Property I is thus obtained:

Property I(a)

If two geometrically similar solids have their entire boundaries held at fixed temperature distributions such that temperatures at corresponding points of the two boundaries are equal then the temperatures at corresponding points throughout the two solids are equal. When the two solids are placed in perspective their two isothermal surfaces corresponding to any given temperature are in perspective, with the same ratio α of perspectivity as the boundaries.

This raises the interesting question of the relation between corresponding isothermal surfaces in geometrically similar solids subject to more general surface temperature conditions. It is just recently that the examination of the nature of families of isotherms for variable temperatures was begun.[3]

It is important to note that the proof of Property IV is independent of the shape of the solid and the amount of its surface area which is exposed to the gas. Suppose, for example, that a slender solid cylinder with length L and diameter D has its entire surface, except for one base, held at a fixed high temperature, while the other base is exposed to cool air at fixed temperature. Consider a second cylinder with dimensions $L'=5L$, $D'=5D$ subject to the same surface temperature conditions. Let P_1 be a point in the small cylinder at a small distance c from the lateral surface and at an equal distance from that base whose temperature is fixed. In the large cylinder the corresponding point P_2 is at a distance $5c$ from the corresponding surfaces. According to Property IV, the steady temperature at P_2 is lower than that at P_1.

This result becomes even less evident intuitively if the cylinders are replaced by two similar truncated cones with only their small bases exposed to cool air. Other more complex shapes illustrate still better the possible deviations of the results of Property IV from the expected results.

In Property V, $h=E/K$ where E is the external conductivity and K is the thermal conductivity. Hence if Newton's law (10) applies, Properties I, II, III can be stated easily in terms of K for a fixed E as well as in terms of the emissivity h.

The linear relation (9) is a convenient one to

[3] E. Kasner, *Geometry of the Heat Equation*, Proc. Natl. Acad. Sci. **18**, 475–480 (1932). Also see abstracts of papers by Kasner (p. 811), Comenetz (p. 803), and Fialkow (p. 803), in the Bulletin of the American Mathematical Society, **38** (1932).

use to determine the applicability of Newton's law in a physical problem. If measurements of T at a fixed point are plotted against measured values of T_g with T_0 fixed, or against values of T_0 with T_g fixed, the deviation of these points from a straight line means deviation from Newton's law.

It is evident that two sets of corresponding values of T_g and T, where T is measured at a fixed point, say the hottest point, determine the values of T_0 and W. Thus in a problem of design the values of T_0 and W may be determined by the extreme values allowable for T and T_g. A body which has this value for W at its hottest point may be obtained by adjusting either the size, shape, or thermal coefficients. According to Properties II and IV however, any value of the relative temperature W made possible by adjusting thermal coefficients can also be obtained by adjusting the size of the body. That is, for given extreme allowable temperatures and given thermal coefficients there is in general an optimum size for any shape rather than an optimum shape.

Stress Distribution in Wedges with Arbitrary Boundary Forces*

J. H. A. BRAHTZ, *Aeronautics Department, California Institute of Technology*

(Received December 20, 1932)

Stress distribution under plain strain in a corner of any angular magnitude. A generalization of the method of von Kármán, applicable to the wedge, for any force distribution over the straight boundaries is outlined. In the first application the stress function is found for a concentrated force acting at any point of the boundaries of the three-quarter plane. Certain stresses are plotted. The stress functions are given without mathematical details for the following boundary conditions in the three-quarter plane: (a) Uniform tension over a part of the boundary; (b) linear distribution over a part of the boundary; (c) superposition of (a) and (b), giving hydrostatic distribution, with a plot of certain stresses. The discussion contains the stress functions for uniform continuous tension on one or both boundaries and points out the very interesting paradox that stresses may be finite for certain continuous loadings, but become infinite if a portion of the load is removed.

I. INTRODUCTION

THE knowledge of two-dimensional stress distributions is useful for the solution of many problems in mechanical and civil engineering, when the usual methods of strength of materials are not applicable or not sufficiently accurate. The stress distribution in the half-plane under the influence of a concentrated force acting on the straight boundary is of fundamental importance, and the solution of this problem is due to Boussinesq. Several extensions of his results have been made by Michell,[1] especially by means of the so-called method of inversion, the only conformal transformation of bi-harmonic solutions which leaves the boundary stresses undisturbed. By superposition of Boussinesq's solutions the stress distribution in the half-plane is easily obtained for an arbitrary load distribution along the straight boundary.

The stress distribution in a plane strip has been discussed by several authors and special reference is made to a paper by Dr. Th. von Kármán[2] containing a general method for the determination of the stresses due to an arbitrary load along the boundaries. The paper is not yet available in the English language, therefore a brief description shall be given of v. Kármán's formulation of the problem.

A two-dimentional elastic system[3] is in equilibrium if the stresses σ_x, σ_y and τ are the second partial derivatives of an arbitrary function $F(xy)$:

$$\sigma_x = \partial^2 F/\partial y^2;\ \sigma_y = \partial^2 F/\partial x^2;\ \tau_{xy} = -\partial^2 F/\partial x \partial y. \quad (1)$$

In order to be compatible with the stress-strain relations in accordance with Hooke's law, F must be a solution of the equation

$$\partial^4 F/\partial x^4 + 2\partial^4 F/\partial x^2 \partial y^2 + \partial^4 F/\partial y^4 = 0$$

or in Gibbs' notation

$$\nabla^4 F = 0. \quad (2)$$

F, known as Airy's function, and its first partial derivatives can be interpreted in terms of the quantities usually employed and defined in "strength of materials," namely, shear and moment of the external forces. By integrating (1) along the boundary between points A and B it is seen that the differences

$$(\partial F/\partial x)_B - (\partial F/\partial x)_A \quad \text{and} \quad (\partial F/\partial y)_B - (\partial F/\partial y)_A$$

represent respectively the resultant Y and X components of the load on the boundary between A and B and, by integrating once more, it is seen that the difference $(F)_B - (F)_A$ represents the increase in the bending moment, in going from A to B.[4]

* Excerpt from Doctor s thesis by the author.

[1] A. E. H. Love, *Elasticity*, page 216.

[2] v. Kármán, *Aachen Abhandlungen*, 1927, p. 7.

[3] See Apendix I.

[4] See: Riemann-Weber, *Differentialgleichungen der Physik*, II.

Hence, if all loads are assumed applied at the upper surface of the strip, x-axis (see Fig. 1), the usual moment curve becomes identical with $F(x, 0)$ for the strip in question and the problem of stress distribution becomes simply the determination of $F(x, y)$ for given boundary values.

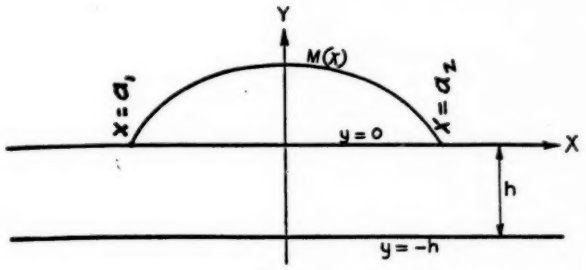

FIG. 1.

It can easily be verified that the following functions are particular integrals of (2):

$A_1 \cos mx \operatorname{Cosh} my$, $A_5 y \cos mx \operatorname{Cosh} my$,
$A_2 \cos mx \operatorname{Sinh} my$, $A_6 y \cos mx \operatorname{Sinh} my$,
$A_3 \sin mx \operatorname{Cosh} my$, $A_7 y \sin mx \operatorname{Cosh} my$,
$A_4 \sin mx \operatorname{Sinh} my$, $A_8 y \sin mx \operatorname{Sinh} my$,

and if we consider the coefficients A_1 etc., functions of the parameter m the Airy's stress function can be written:

$$F=\int_0^\infty [(A_1 \operatorname{Cosh} my+A_2 \operatorname{Sinh} my+A_5 y \operatorname{Cosh} my +A_6 y \operatorname{Sinh} my) \cos mx+(A_3 \operatorname{Cosh} my +A_4 \operatorname{Sinh} my+A_7 y \operatorname{Cosh} my +A_8 y \operatorname{Sinh} my) \sin mx]dm, \quad (3)$$

where A_1, etc., are to be determined by the boundary conditions.

If the depth of the beam is h, the boundary conditions to be satisfied by F are: $\partial F/\partial y=0$, $F=M(x)$ at the upper boundary, $y=0$; $\partial F/\partial y=0$, $F=0$ at the lower boundary, $y=-h$. As in Fig. 1, the moment $M(x)$ is assumed to be zero except in the region $x=a_1$ to $x=a_2$ and we now express $M(x)$ as a Fourier integral:

$$M_x=\int_0^\infty (a \cos mx+b \sin mx)dm,$$

where a and b are determined by

$$a=\frac{1}{\pi}\int_{a_1}^{a_2} M(\alpha)\cdot \cos m\alpha d\alpha,$$

$$b=\frac{1}{\pi}\int_{a_1}^{a_2} M(\alpha) \sin m\alpha d\alpha.$$

We now form the four boundary equations which must hold for all values of x. Hence, by equating to zero the coefficients of $\cos mx$ and $\sin mx$ we obtain eight other equations which determine the coefficients A_1, etc. (later in this paper this process is carried out in detail), and by the substitution of these in (3) we finally obtain the stress function F. By (1) the stresses are then found.

In other words, if it is possible to represent the moment distribution $M(x)$ as a Fourier's integral the solution of the stress problem is immediately obtained.

v. Kármán and F. Seewald have applied this method to several important cases and obtained interesting results, among others the "corrected" relation between the bending moment and shear at a point of a beam and the curvature of the central line

$$K(M/EI)+[6/5G-9\mu/10E](P/A), \quad (4)$$

where K denotes the curvature, E and G Young's modulus and the corresponding modulus in shear, Poisson's ratio, A area of cross section, I moment of inertia, M and P the bending moment and shear at the point in question. The second term corresponds to the influence of shear on the deflection.

A new and interesting conclusion of this theory is that the deflection of the central line of a long beam is wave shaped outside the loaded region.

II. Solutions for Arbitrary Boundary Loads on a Wedge

The method described above can be applied to any angular portion (γ) of the plane with any distribution of both normal and tangential forces over the straight boundaries.

Introducing polar coordinates and stress function must satisfy the equation

$$\nabla^4 F(r, \theta)=(\partial^2/\partial r^2+\partial/r\partial r+\partial^2/r^2\partial\theta^2)^2 F=0 \quad (5)$$

with corresponding stresses, see Fig. 2:

$$\sigma_r=\partial^2 F/r^2\partial\theta^2+(1/r)(\partial F/\partial r), \quad (6)$$

$$\sigma_\theta=\partial^2 F/\partial r^2, \quad (7)$$

$$\tau=-(\partial/\partial r)(\partial F/r\partial\theta). \quad (8)$$

For the present purpose we will employ the functions obtained by taking real and imaginary parts of

$$\varphi_n = \tfrac{1}{2} \cdot (x \text{ and } y) \cdot (z^{im} \pm z^{-im}), \qquad (9)$$

where m is real and to be determined by the boundary conditions.

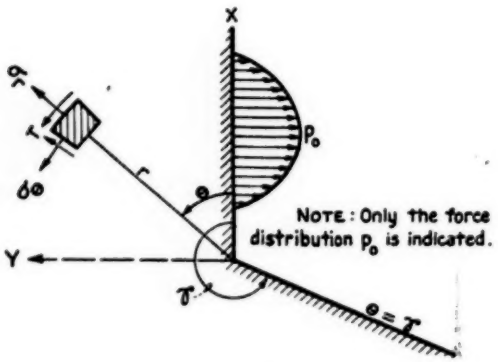

FIG. 2.

We obtain the following particular solutions of $\nabla^4 F = 0$:

$$\begin{aligned}
&\varphi_1 = x\cos m\xi \operatorname{Cosh} m\theta, && \varphi_5 = y\cos m\xi \operatorname{Cosh} m\theta,\\
&\varphi_2 = x\cos m\xi \operatorname{Sinh} m\theta, && \varphi_6 = y\cos m\xi \operatorname{Sinh} m\theta,\\
&\varphi_3 = x\sin m\xi \operatorname{Sinh} m\theta, && \varphi_7 = y\sin m\xi \operatorname{Sinh} m\theta,\\
&\varphi_4 = x\sin m\xi \operatorname{Cosh} m\theta, && \varphi_8 = y\sin m\xi \operatorname{Cosh} m\theta,
\end{aligned} \qquad (9a)$$

where $\xi = \log r$.

The coefficients A_n are now defined as functions of the parameter m. The stress function may then be expressed as

$$F = \sum_{n=1}^{n=8} \int_0^\infty A_n(m) \cdot \varphi_n \cdot dm$$

$$= \int_0^\infty [A_1\varphi_1 + A_2\varphi_2 + \cdots A_8\varphi_8] dm, \qquad (10)$$

from which the stresses are obtained by (6), etc.

Two typical cases of boundary loads must be considered:

(a) *The load may be continuous (not necessarily uniform) over portions of the straight boundaries.* Let it be assumed that the load is distributed over finite portions of the boundaries or, if the load extends to infinity, that the load per unit length becomes zero at infinity. Let the boundaries be the lines $\theta = 0$ and $\theta = \gamma$, and let the normal loads be respectively p_0 and p_γ and the tangential loads be q_0 and q_γ. These quantities are functions of r, measured from the intersection of the boundaries, or functions of $\xi = \log r$. Using Fourier's double integrals, we can write $p_0(\xi)$ in the following form[5]:

$$p_0(\xi) = \frac{1}{\pi}\int_0^\infty \left[\cos m\xi \int_{\xi_1}^{\xi_2} p_0(\alpha)\cdot\cos m\alpha d\alpha + \sin m\xi \int_{\xi_1}^{\xi_2} p_0(\alpha)\cdot\sin m\alpha d\alpha\right] dm, \qquad (11)$$

where the load $p_0(\xi)$ is assumed to exist only between the points ξ_1 and ξ_2. Similar expressions are obtained for p_γ, q_0 and q_γ. Therefore, the boundary conditions are

$$(\sigma_\theta)_{\theta=0} = p_0(\xi) \text{ expressed as in (11)} \qquad (12)$$

$$(\tau)_{\theta=0} = q_0, \qquad (13)$$

$$(\sigma_\theta)_{\theta=\gamma} = p_\gamma, \qquad (14)$$

$$(\tau)_{\theta=\gamma} = q_\gamma, \qquad (15)$$

where σ_θ and τ are given by (7) and (8).

By now equating to zero the coefficients of $\cos m\xi$ and $\sin m\xi$ in the above equations, eight other equations are obtained which determine the eight functions $A(m)$ and consequently the stress function F by substituting $A_n(m)$ in (10).

(*b*) In the case of concentrated loads the boundary conditions are obtained in the following manner: It was already shown that the differences $(\partial F/\partial x)_B - (\partial F/\partial x)_A$ and $(\partial F/\partial y)_B - (\partial F/\partial y)_A$ represent, respectively, the Y and X components of all the boundary forces between A and B. Therefore, in the case of concentrated forces, these differences become discontinuous (similar to the shear polygon for concentrated forces) and the jump in these values at a certain point is equal to the respective components of the concentrated force at that point. Consider for instance unit normal force acting at point $r = a$ of the boundary $\theta = 0$. Obviously $(\partial F/\partial r)_{a+\epsilon} - (\partial F/\partial r)_{a-\epsilon} = 1$, where ϵ is a small positive quantity. If there is no continuously distributed load on the boundary $\theta = 0$, then by (12) $(\sigma_\theta)_0 = (\partial^2 F/\partial r^2)_0 = 0$.

Hence $\partial F/\partial r$ is a constant on either side of

[5] See *Fourier Series* by W. E. Byerly.

$r=a$. These conditions can all be satisfied by writing[6]

$$\frac{\partial F}{\partial r}=\frac{1}{\pi}\int_0^\infty \frac{\sin(m\xi)}{m}\,dm. \tag{16}$$

This integral has the value $-\frac{1}{2}$ for $\xi=\log(r/a)<0$ or $r<a$ and $+\frac{1}{2}$ for $\xi>0$ or $r>a$. The integral[7]:

$$\frac{1}{\pi}\int_0^\infty \frac{n\cos m\xi - m\sin m\xi}{m^2+n^2}\,dm=\begin{cases} e^{n\xi} \text{ when } \xi<0,\\ \frac{1}{2} \text{ when } \xi=0,\\ 0 \text{ when } \xi>0, \end{cases} \tag{17}$$

with its ramifications is often very useful in expressing boundary functions on Fourier integral form. (See Fig. 3.)

III. Application

In the first application of the foregoing, the stress function F corresponding to a unit normal traction at point $r=a$ of boundary $\theta=0$ will be found for a reentrant right corner, i.e., $\gamma=3\pi/2$.

The boundary conditions are when $\theta=0$: $\partial F/\partial r=0$ when $\xi\equiv\log(r/a)\lessgtr 0$, $\partial F/\partial r=1$ when $\xi>0$, $\partial F/\partial\theta=0$; when $\theta=\gamma$: $F=0$, $\partial F/\partial\theta=0$. Let $F=F_0+F_1$. F_0 is determined by the boundary conditions

$$(\partial F_0/\partial r)_0=-\tfrac{1}{2} \text{ for } \xi<0, =+\tfrac{1}{2} \text{ for } \xi>0$$

$$(\partial F_0/\partial\theta)_0=0,\ (F_0)_\gamma=0,\ (\partial F_0/\partial\theta)_\gamma=0.$$

Hence by Eq. (16),

$$\left(\frac{\partial F_0}{\partial r}\right)_0=\frac{1}{\pi}\int_0^\infty \frac{\sin m\xi}{m}\,dm,$$

In order to remove the concentrated force introduced at the origin (because of the discontinuity in the first derivative) F_1 is determined so that $(\partial F_1/\partial r)_0=\frac{1}{2}$ for $-\infty\lessgtr\xi\lessgtr+\infty$; $(\partial F_1/\partial\theta)_0=(F_1)_\gamma=(\partial F_1/\partial\theta)_\gamma=0$. F_1 is easily found by employing the simple solution to $\nabla^4F_1=0$:

$$F_1=A\theta r\cos\theta+B\theta r\sin\theta + Cr\cos\theta+Dr\sin\theta. \tag{18}$$

Hence, by the boundary conditions for F_1: $(\partial F_1/\partial r)_0=C=\frac{1}{2}$; $(\partial F_1/\partial\theta)_0=Ar+Dr=0$; $(F_1)_\gamma=-(3\pi/2)Br-Dr=0$; $(\partial F_1/\partial\theta)_\gamma=(3\pi/2)Ar-Br+Cr=0$. Solving these and substituting in (18) we obtain

$$F_1=[r\theta/(4-9\pi^2)](3\pi\cos\theta+2\sin\theta). \tag{19}$$

The first degree terms have been omitted as they contribute no stress.

In order to determine F_0 we employ Eq. (10) and formulate the given boundary conditions by differentiating the functions given by (9a) and obtain:

$$\left(\frac{\partial F_0}{\partial r}\right)_0=\int_0^\infty [A_1(c-ms)+A_4(mc+s)]dm = \frac{1}{\pi}\int_0^\infty \frac{s}{m}\,dm,$$

$$\left(\frac{\partial F_0}{r\partial\theta}\right)_0=\int_0^\infty [mA_2c+mA_3s+A_5c+A_8s]dm=0,$$

$$(F_0)_\gamma=\int_0^\infty [-mA_5Cc-A_6Sc-A_7Ss - A_8Cs]dm=0,$$

$$\left(\frac{\partial F_0}{r\partial\theta}\right)_\gamma=\int_0^\infty [A_1Cc+A_2Sc+A_3Ss+A_4Cs - mA_5Sc-mA_6Cc-mA_7Cs-mA_8Ss]dm=0,$$

where $C=\operatorname{Cosh}\gamma m$, $S=\operatorname{Sinh}\gamma m$, $c=\cos m\xi$, $s=\sin m\xi$. By equating the coefficients of c and s to zero we obtain the eight equations:

$$A_1+mA_4=0;\quad -mA_1+mA_4=1/\pi m;$$

$$mA_2+A_5=0;\quad mA_3+A_8=0;\quad CA_5+SA_6=0;$$

$$-SA_7-CA_8=0;\quad CA_1+SA_2-mSA_5-mCA_6=0;$$

$$SA_3+CA_4-mCA_7-mSA_8=0;$$

and solving:

$$A_1=-m(S^2-m^2)\Lambda;\quad A_5=-m^2CS\Lambda;$$

$$A_2=+CSm\Lambda;\quad A_6=+m^2C^2\Lambda;$$

$$A_3=-CS\Lambda;\quad A_7=-mC^2\Lambda;$$

$$A_4=+(S^2-m^2)\Lambda;\quad A_8=+mCS\Lambda;$$

where $\Lambda=1/\pi m(1+m^2)(\operatorname{Sinh}^2\gamma m-m^2)$.

The stress function is then found simply by substituting the A's back into Eq. (10). The stress-function in the $\frac{3}{4}$-plane for unit tensile force concentrated at the point $(r,\theta)=(a,0)$ becomes after some reduction $F=F_0+F_1$.

[6] See Peirce, *Short Tables of Integrals*, No. 484.

[7] Riemann-Weber, *Differentialgleichungen der Physik*, I, page 157.

$$F=\int_0^\infty [m^2x\,\mathrm{Cosh}\,m\theta-(xS+myC)\,\mathrm{Sinh}\,m(\gamma-\theta)]\cdot(mc-s)\Lambda dm+[r\theta/(4-9\pi^2)](3\pi\cos\theta+2\sin\theta). \quad (20)$$

The integral F may be evaluated by the method of contour integration in the complex plane,[8] by making use of Cauchy's theorem of residues as outlined in the appendix.

The stress functions evaluated in this manner valid for small and large values of $|\xi|$ become: $F_0+F_1=$

$$F=a[0.101(r/a)^{1.545}g(\theta)+0.125(r/a)^{1.909}h(\theta)] \quad \text{when } r/a\ll 1, \quad (28)$$

$$F=-a[0.340(r/a)^{0.455}g(\theta)+2.629(r/a)^{0.091}h(\theta)]+[2r\theta/(4-9\pi^2)](3\pi\cos\theta+2\sin\theta)-a\cos^2\theta \quad \text{when } r/a\gg 1, \quad (29)$$

where

$$g(\theta)=\sin(0.545\theta)\cos\theta-0.545\cos(0.545\theta)\cdot\sin\theta-0.839\sin(0.545\theta)\sin\theta, \quad (30)$$

$$h(\theta)=\sin(0.909\theta)\cos\theta-0.909\cos(0.909\theta)\cdot\sin\theta+0.416\sin(0.909\theta)\sin\theta. \quad (31)$$

It is interesting to notice that the terms in (28) including those of higher order are the biharmonic functions of the wedge (solutions of $\nabla^4F=0$) which correspond to boundaries free of forces. This can also be seen by writing

$$F=Ar^n\cos n\theta+Br^n\cos(n-2)\theta+Cr^n\sin n\theta+Dr^n\sin(n-2)\theta, \quad (32)$$

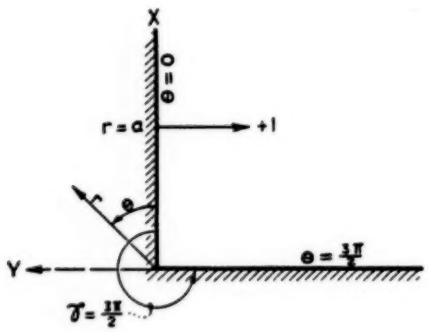

FIG. 3.

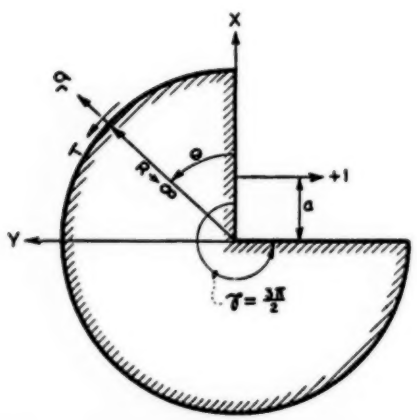

FIG. 4.

where n may be complex and finding the values of n which give possible solutions in case F and $\partial F/\partial\theta$ are both to be zero along both boundaries. The determinant of the four boundary equations gives exactly the roots corresponding to the exponents in (28). It is, however, only possible to determine the ratios B/A, etc., in this way. The absolute values of the constants naturally depend upon the location and magnitude of the concentrated forces, and these can only be specified by the use of Fourier integrals as above.

The writer is informed that Dr. H. M. Westergaard, Professor of Theoretical and Applied Mechanics, University of Illinois, in a communication to Dr. Th. von Kármán, has pointed out the existence of these solutions.

Check on boundary conditions: By (28) and (29) it is easily verified that

$$F=0\left\{\begin{array}{l}\text{when } \theta=0\\ \text{and } \theta=3\pi/2\end{array}\right.$$
$$\partial F/\partial\theta=0$$

are satisfied.

In order to investigate if all boundary forces are in equilibrium we will determine the stresses on a circle of large radius $r=R$ (see Fig. 4). By differentiating (29) and only taking such terms that contribute: as $r=R\to\infty$,

$$\sigma_r=(12\pi\sin\theta-8\cos\theta)/(9\pi^2-4)R,$$

$$\tau=a\sin 2\theta/R^2.$$

[8] See for explanation Mac Robert, *Functions of a Complex Variable.*

Projecting on x-axis and letting $R\to\infty$:

$$\sum X=\int_0^\gamma rd\theta\,\sigma_r\cos\theta=0.$$

Projecting on Y-axis:

$$\sum Y=\int_0^\gamma rd\theta\,\sigma_r\sin\theta=1.$$

Moments about the origin:

$$M_0=\int_0^\gamma \tau r^2d\theta=\left[-\tfrac{1}{2}a\cos 2\theta\right]_0^\gamma=+a.$$

It will be seen that all equilibrium conditions are satisfied, the only other force being unit tensile force at a. The stresses for large and small radii are now obtained from (28) and (29) by application of Eqs. (6), (7) and (8). It will be noticed that stresses become infinite at the origin.

Evaluation of stresses

If it is only desired to know the stresses at certain points or the distribution on a line it is often simpler to specialize F in (20) before evaluating the integral.

For example, to obtain the distribution of normal stress on the Y-axis, place $\theta=\pi/2$ in (20):

$$F=-\frac{r}{\pi}\int_0^\infty\frac{\text{Cosh}\,\gamma m\cdot\text{Sinh}\,\pi m}{(1+m^2)(\text{Sinh}^2\gamma m-m^2)}(m\cos m\xi-\sin m\xi)dm+F_1, \tag{33}$$

$$\sigma_\theta=\frac{\partial^2F}{\partial r^2}=\frac{1}{\pi r}\int_0^\infty\frac{m\,\text{Cosh}\,\gamma m\cdot\text{Sinh}\,\pi m}{\text{Sinh}^2\gamma m-m^2}\cos m\xi dm. \tag{34}$$

Notice that F_1 contributes nothing.

By (28) and (29) we obtain the correct stresses for small and large radii which usually are the most interesting, so that only a few additional terms of higher powers in r would be needed to give the stresses in the region $r=a$. These can be obtained by the method of residues applied to (34) as explained above. However, if only a plot of stresses is desired, it is simpler to evaluate (34) for values of r in the neighborhood of a, by more primitive methods. The simplest of these would perhaps be to plot the integrand for various values of m and r and apply Simpson's rule. This need only be done for $m\lessapprox 1$ because for larger m, (34) can be further simplified by placing $\text{Cosh}\,m\gamma=\text{Sinh}\,m\gamma=e^{3\pi m/2}$ and ignoring m^2 in the denominator. The integral then becomes

$$\frac{1}{\pi r}\int^\infty me^{-\pi m/2}\cos m\xi dm.$$

The stresses σ_θ obtained by evaluating (34), are plotted in Fig. 5. The corresponding stresses for the half-plane, $\gamma=\pi$, are also shown. It is interesting to notice the effect of the additional quarter plane by comparing the two stress distributions, I and II. Boussinesq's solution for a unit traction at $x=a$ on the x-axis gives

$$\sigma_x=(2/\pi a)(y/a)/[1+(y/a)^2]^2 \tag{35}$$

along the Y-axis, which is plotted as the curve II of Fig. 5.

If several concentrated forces are applied on the boundary $\theta=0$, the stress functions and stresses are obtained by superposing the functions computed for the various values of a. For a concentrated force acting on the boundary $\theta=3\pi/2$, the stresses are obtained from the above formulae by substituting $\theta=(3\pi/2)-\theta$ for θ, maintaining the same coordinate system.

It is of interest to note that the function $g(\theta)$ given in (30) is symmetric and $h(\theta)$ given in (31) is antisymmetric about the bisector of the angle γ. This holds also for the corresponding functions for higher powers in r/a. This would mean that concentrated forces of equal magnitude located on each boundary at equal distance from the vertex would have stress functions (valid near the vertex):

$$F=0.202a(r/a)^{1.545}\cdot g(\theta) \tag{28a}$$

if the unit forces are both tension and

$$F=0.250a(r/a)^{1.909}\cdot h(\theta) \tag{29a}$$

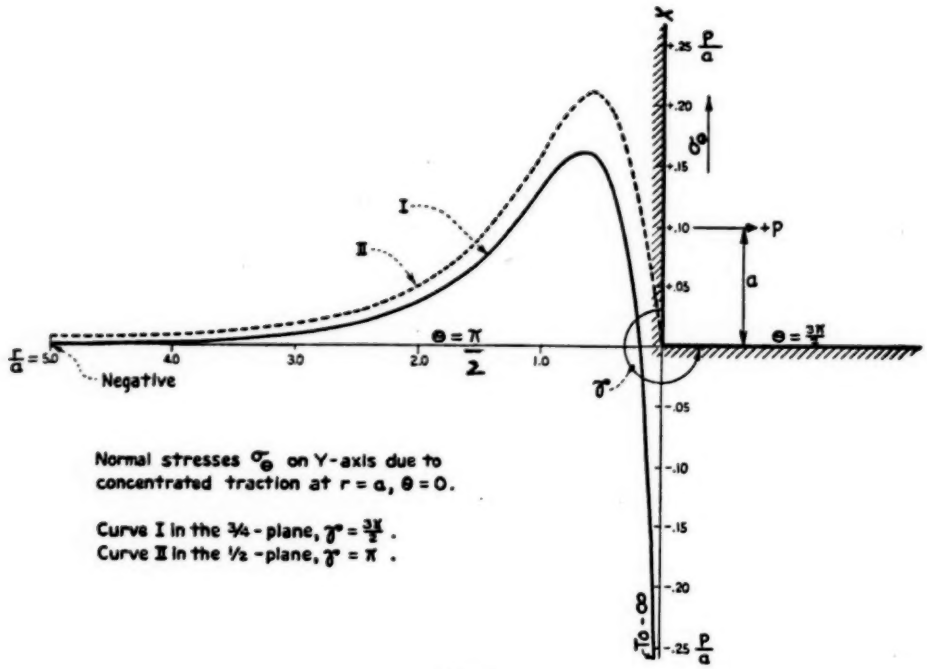
Normal stresses σ_θ on Y-axis due to concentrated traction at r = a, θ = 0.
Curve I in the ¾ - plane, $\gamma^\circ = \frac{3\pi}{2}$.
Curve II in the ½ - plane, $\gamma^\circ = \pi$.
Negative
I
II
+P
a

FIG. 5.

with traction on the boundary $\theta=0$ and pressure on $\theta=3\pi/2$. This shows that the stress at the vertex is always infinite for partial loading of the boundaries.

IV. ADDITIONAL RESULTS

Other types of boundary conditions for a right reentrant corner have been studied the results of which shall be stated here omitting the mathematical details.

(a) With uniform tension p on the boundary $\theta=0$ between points $r=0$ and $r=a$

$$F=ap\left\{\int_0^\infty [-m^2x\ \mathrm{Cosh}\ m\theta+(xS+myC)\ \mathrm{Sinh}\ m(\gamma-\theta)]s\Lambda dm+\frac{r\theta}{4-9\pi^2}[3\pi\cos\theta+2\sin\theta]\right\}. \quad (36)$$

(b) With linear tension pr on the boundary $\theta=0$ between the points $r=0$ and $r=a$:

$$F=ap\left\{\int_0^\infty [m^2x\ \mathrm{Cosh}\ m\theta-(xS+myC)\ \mathrm{Sinh}\ m(\gamma-\theta)]\cdot[mc-(m^2+2)s]\Lambda dm + \frac{r\theta}{2(4-9\pi^2)}[3\pi\cos\theta+2\sin\theta]\right\}. \quad (37)$$

(c) By superposition of a and b we obtain the stress function for hydrostatic loading (tension)

$$F=ap\left\{\int_0^\infty [-m^2x\ \mathrm{Cosh}\ m\theta+(xS+myC)\ \mathrm{Sinh}\ m(\gamma-\theta)]\cdot(mc+2s)\Lambda\cdot dm + \frac{1}{2}\frac{r\theta}{4-9\pi^2}(3\pi\cos\theta+2\sin\theta)\right\}. \quad (38)$$

In Fig. 6 the normal stresses on the line $\theta=\pi/2$ because of hydrostatic loading are plotted. Curve II shows the same stresses for similar loading on the half plane ($\gamma=\pi$).

It will be noticed that Eq. (23) in the Appendix has no real roots, except $m=0$, when γ is less than π. This means that in general a partial loading of the boundaries of a corner will produce finite stresses at the origin (vertex) if $\gamma<\pi$, but infinite stresses if $\gamma>\pi$, and the greater γ is the sharper the infinity. The half-plane, $\gamma=\pi$, thus is the critical case and the stresses at the origin are zero if it is chosen outside the loaded region.

Special cases of stress distribution in an infinite wedge have been treated by a number of investigators. We find J. H. Michell[9] who generalizes Boussinesq's solution for a concentrated force on the half-plane to a concentrated force at the vertex of an infinite wedge, M. Levy[9] who finds a solution for a linear load distribution over the boundaries, S. D. Carothers[10] who gives solutions for a couple at the vertex and uniform loads on the boundaries.

The stress function for continuous uniform pressure on the boundaries is easily determined by Eq. (32).

$$F=-\tfrac{1}{2}pr^2\cos^2\theta \qquad (39)$$

corresponds to uniform pressure on the boundary $\theta=0$. It will be seen that the stresses are finite at the vertex for any value of γ. We have seen that a partial loading produces infinite stress at the vertex if $\gamma>\pi$, so that we have the curious result that in this case the removal of a portion of the load raises the stress to infinity.

If uniform pressure acts on the boundary $\theta=3\pi/2$ the corresponding stress function is

$$F=-\tfrac{1}{2}pr^2\sin^2\theta. \qquad (40)$$

In Fig. 6 is plotted the normal stresses on the base, $\theta=\pi/2$, due to linear pressure distribution on the boundary, $\theta=0$. It is important to notice that near the vertex the base is under high tension.

Levy's solution for linear normal pressure on the boundary of an infinite wedge (or triangle) shows linear distribution of all stresses along any straight line through the wedge. In practice this result is conveniently applied to masonry dams. However, the application is dubious because the height of a dam is of the same order of magnitude as the base width, so that

[9] A. E. H. Love, *Elasticity*, page 212.
[10] Proc. Roy. Soc. (Edin.) **53**, 292 (1913).

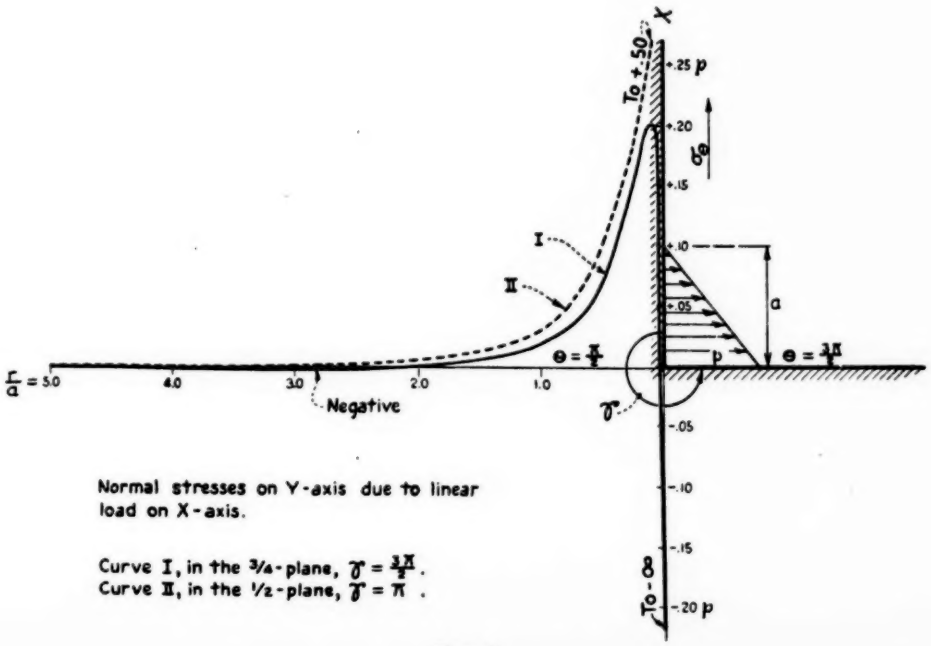

FIG. 6.

great deviations from the linear stress distribution can be expected (at any rate near the base) because of the influence of the unyielding, or rather, infinite foundation.

Engineers are well aware of this fact, and the present study grew out of an attempt to determine the stress distribution in triangular dams on infinite, rigid and elastic foundations by the Ritz' method. However, it was found that the stresses in the up- and downstream faces at the base did not converge when more parameters were included in the solution. At points only slightly distant from the up- and downstream corners Ritz' method gave reasonable results.

The present method enables us to compute the stresses in dams of triangular and other shapes for any load and far more accurate solutions may be reached in this manner.

Photoelastic experiments are at present being carried out at the California Institute by the author for the purpose of verifying the theoretical results of this study. It is of special interest to find out how closely the equation $\nabla^4 F=0$ holds for plates of finite thickness. The stress distribution is also being investigated in plates of arbitrary shapes, especially applicable to masonry dams, also the stress concentrations around openings corresponding to the inspection and drainage galleries which usually exist in high dams and finally the stresses caused by temperature changes and chemical shrinkage.

The author wishes to express his appreciation to Dr. Th. von Kármán, Director of the Guggenheim Graduate School of Aeronautics, and Dr. Harry Bateman, Professor of Mathematics, California Institute of Technology, for their valuable suggestions in the carrying out of this study and investigations.

Appendix

Evaluation by Contour Integration

Cauchy's theorem of residues

$$\oint_S \Psi(m)dm = 2\pi i \cdot (\text{Sum of residues})$$

enables us to compute the definite integral in (20). m is complex $=\alpha+i\beta$. The residues are found by integrating around each pole in the positive direction. F_0 may be written as

$$F_0=\frac{1}{2\pi}\int_{-\infty}^{+\infty}\frac{m\cdot f(m)\cdot\cos m\xi dm}{m(1+m^2)(\operatorname{Sinh}^2\gamma m-m^2)}-\frac{1}{2\pi}\int_{-\infty}^{+\infty}\frac{f(m)\cdot\sin m\xi dm}{m(1+m^2)(\operatorname{Sinh}^2\gamma m-m^2)}=M_1-M_2,$$

where the meaning of $f(m)$ is evident by comparing with Eq. (20).

Consider the complex integrals:

M_2 = The imaginary part of

$$\frac{1}{2}\oint e^{im\xi}\cdot f(m)\Lambda dm \qquad (21)$$

M_1 = The real part of

$$\frac{1}{2}\oint_S m\cdot e^{im\xi}\cdot f(m)\Lambda dm \qquad (22)$$

taken along the contours S consisting of the real axis and the infinite half circle above or below the real axis, see Fig. 7.

If $\xi\equiv\log(r/a)<0$ the half circle below the real axis must be chosen because in this case the integral along this part of the path converges to zero as $m\to\infty$. For the same reason the upper infinite half circle is chosen when $\xi>0$, i.e., $r>a$.

Consider for example the lower half-plane: Let $m=\alpha-i\beta$ where β is real and positive, then, if $0>\xi=-c$ where c is real and positive,

$$e^{im\xi}=e^{i(\alpha-i\beta)(-c)}=e^{-ic\alpha}\cdot e^{-c\beta}\frac{\cos\alpha c-i\sin\beta c}{e^{c\beta}},$$

which becomes zero in the limit.

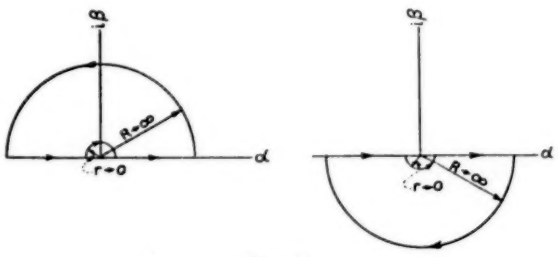

Fig. 7.

The singularities of the integrand are all simple poles and are the roots of:

$$\operatorname{Sinh}^2\gamma m-m^2=0 \qquad (23)$$

or if m is pure imaginary $i\beta$

$$\beta = \pm \sin(\gamma\beta). \tag{24}$$

The complex roots may be found with very good approximation (except $n=2$) by:

$$m=\alpha_n+i\beta_n= \pm \frac{1}{\gamma}\log\frac{\pi(2n+1)-\epsilon}{\gamma} \pm i\frac{(2n+1)-\epsilon}{2\gamma}, \tag{25}$$

where

$$\epsilon = 4\log[(2n+1)/\gamma]/\pi(2n+1) \tag{26}$$

and $n=2, 3, 4, 5. \ldots \infty$; $\gamma=3\pi/2$. For large values of n:

$$m=\alpha_n+i\beta_n= \pm\frac{2}{3\pi}\log\frac{4n+2}{3} \pm i\frac{2n+1}{3}. \tag{27}$$

The lower roots are:

α:	0	0	0	0	± 0.231	± 0.320
β:	0	± 0.539	± 0.909	± 1	± 1.629	± 2.303

where 1.629 corresponds to $n=2$ in (25) and 2.303 corresponds to $n=2$.

It will be seen that for $|m| \leqq 1$ the roots are located on the imaginary axis, i.e., pure imaginary. For $|m|>1$ all the roots are complex and located near the imaginary axis.

The convergence of the power series is rapid and even for values of r near a, only a few of the poles need be considered outside the unit circle $|m|=1$. For very large $|\xi|$ only the poles inside the circle $|m|=1$ contribute.

Characteristics and Functions of Thyratrons

A. W. HULL, *Research Laboratory, General Electric Company*

(Received January 3, 1933)

The Thyratron is a tube of very low resistance (arc discharge) which can be started or prevented from starting by a grid. Its qualities are: enormous power-amplification, approximately 10^{11} per tube; efficiency between 95 and 99 percent at all voltages above 250; unlimited size, as regards current-capacity; high-voltage limit equal to that of the Pliotron; starting time one to six microseconds; deionization time 10 to 500 microseconds.

Use of Thyratron as switch and for power control. The controlling element may be a switch, clock, thermostat, or photo-tube; the controlled element a motor, magnet, contactor, or reactor. Typical applications of this kind of use are; turning on lamps at dusk, dispatching products to predetermined stations, cutting hot steel bars to exact length, opening doors at the approach of a person, wrapping packages, sorting beans and other articles, counting people or products, operating line or spot welding machines. By varying the phase of the grid-voltage with respect to that of the anode voltage, a smooth variation of *average* anode current may be obtained. A typical application is the dimming and blending of lights in theaters.

Use of Thyratron as rectifier and as inverter from direct to alternating current. Immediate objectives are frequency changing, from 60 to 25 cycles for railway and power purposes, and from 60 to 200 for spinning mills; and commutatorless motors of variable and controllable speed. A more remote but important application is d.c. transmission of power, with inversion to a.c. at the point of utilization.

Use of Thyratrons in scientific research. Applications include high-speed stroboscopes, timing devices, synchronous switches, and voltage regulators. Most interesting and promising of all is a device for counting alpha-particles, protons, and neutrons.

THE Pliotron tube, or electron-tube, as it has come to be called, has reached the stage of familiarity that leaves us leisure to wish for something more. "If only we had a tube which combines the control characteristics of the Pliotron tube with low-resistance and large power capacity," one frequently hears.

THE IDEAL POWER TUBE

But do you want such a tube? Consider how you could use it. You would connect it in series with a resistance or load device of some kind (Fig. 1), and a source of voltage. Assume it to be operating, carrying full load—let it be a typical railway load of 1000 amperes at 500 volts. You now make the grid negative and reduce the current to half. The voltage drop across the load, which was formerly 500, is now 250. Where are the other 250 volts? Obviously in the tube, whose resistance must now be high, high enough to absorb half the voltage and half the power. The grid has reduced the tube current by increasing the tube resistance. There appears to be no other way, for grid modulation of current and low tube resistance are mutually inconsistent. The difficulty is as fundamental as that of the child who finds he cannot have his cake and eat it. We may have either low resistance or continuous control, by a grid, but not both. In large tubes, where power waste is important, the choice must be low resistance. You would not and could not use continuous control by a grid if you had it.

The ideal power valve is therefore one which has low resistance and can be started or stopped by means of a grid. But would you really use the stopping feature? Returning to Fig. 1, let us make the grid more negative than before and completely stop the 1000 amperes. If this is done quickly, there will be no serious dissipation of power in the tube. But what will become of

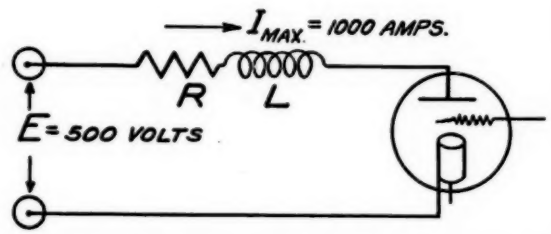

FIG. 1. Typical circuit for grid-controlled power tube. The grid cannot control the magnitude of the current without introducing high resistance in the tube.

the energy, $\frac{1}{2}Li^2$, stored inductively in the motor armature? Physicists familiar with induction coils know the answer. The voltage will rise until all this energy is stored in the capacitance across the tube, or until the insulation fails. It is an axiom among engineers that currents should be "broken" only when they pass through zero. That is, they must be allowed to die naturally, and simply be prevented from restarting. Hence you would not use the stopping feature if you had it.

I think we must conclude that the characteristics desired for our ideal power tube are: low resistance; ability to start at will, by the use of small control-power; and ability to remain nonconducting after stopping.

Description of Thyratron

We have such a tube, with precisely these qualities.[1] It has been named *Thyratron*,* from the Greek word Θύρα, meaning door—the door tube. The Thyratron (Fig. 2) is a grid-controlled arc-discharge device. Its parts are a cathode, either thermionic or mercury pool type; a grid; anode; gas-tight envelope; and an inert gas or vapor, usually argon or mercury, at very low pressure. The pressure varies, in the case of mercury, from 0.001 mm to 0.050 mm, the lower pressure being used for high voltage and rapid deionization, the higher when efficiency and large current capacity are paramount. For argon and helium, the pressures should be about 3 and 10 times higher, respectively. Slightly higher pressures, about twice the above values, may be used at low voltage.

One structural feature deserves mention. It has been found possible to use thermionic cathodes of a special type, which require very little energy to keep them hot.[2] This is accomplished by heat-shielding the cathode on the outside, except for a few small openings, taking advantage of the fact that *electrons in the presence of an equal number of positive ions can flow around corners* and through narrow crevices, with very little resistance, whereas heat radiation must proceed in straight lines. Fig. 3 shows such a cavity cathode, open at one end, but protected from loss of heat over the rest of its surface by several concentric metal cylinders. Inside the cavity are 16 barium-coated vanes, with a total area of 250 cm², and normal electron emission of 75 amperes. The heat-loss is 60 watts. Fig. 4 shows another form of this type of cathode, consisting of a large number of barium-coated nickel disks surrounded by heat-insulating cylinders, with a series of small holes for the escape of electrons. This cathode requires 300 watts to keep it hot and has an electron emission of 600 amperes. An open or unshielded cathode of the same wattage would emit only 15 amperes. It is to be noted that the cavity type of cathode is useful only in tubes containing gas, where space-charge does not limit the flow of electrons.

Now let us consider the properties of this new tube.

Power Amplification

In the first place, it is capable of enormous power amplification, thousands of times greater, even, than the Pliotron.* For example, a typical small Pliotron will give, at best, an increase of 2 milliamperes in plate current for 1 volt change of grid potential. A Thyratron of the same size gives an increase of 2 amperes instead of 2 milliamperes. The power required to change the grid potential is essentially the same in the two cases. This is shown in Fig. 5, which gives the grid current at the instant of starting in an FG-95 Thyratron, rated at 2.5 amperes, 1000 volts. It is seen that the maximum current at starting is 0.005 microampere, at any anode voltage between 200 and 1000. Tests have shown that a resistance of 1000 megohms in series with the grid does not interfere with reliable starting. Hence the input power may be taken as $i^2R=(5\times10^{-9})^2\times10^9=2.5\times10^{-8}$ watts, and the output power at 1000 volts as $EI=1000\times2.5=2.5$ kw. The ratio $(2.5\times10^3)/(2.5\times10^{-8})=10^{11}$, is the power amplification.

The control characteristic of the FG-95 Thyratron is shown in Fig. 6. Its *control ratio* of grid to anode volatge is seen to be about 1/200,

* G. E. Trademark.

[1] A. W. Hull and I. Langmuir, *Control of an Arc Discharge by a Grid*, Proc. Nat. Acad. Sci. **51**, 218–25 (1929). A. W. Hull, *Hot Cathode Thyratrons*, Gen. Elec. Rev. **32**, 213–23, 390–99 (1929).

[2] A. W. Hull, *Gas-Filled Thermionic Tubes*, Trans. A.I.E.E. **47**, 753–63 (1928).

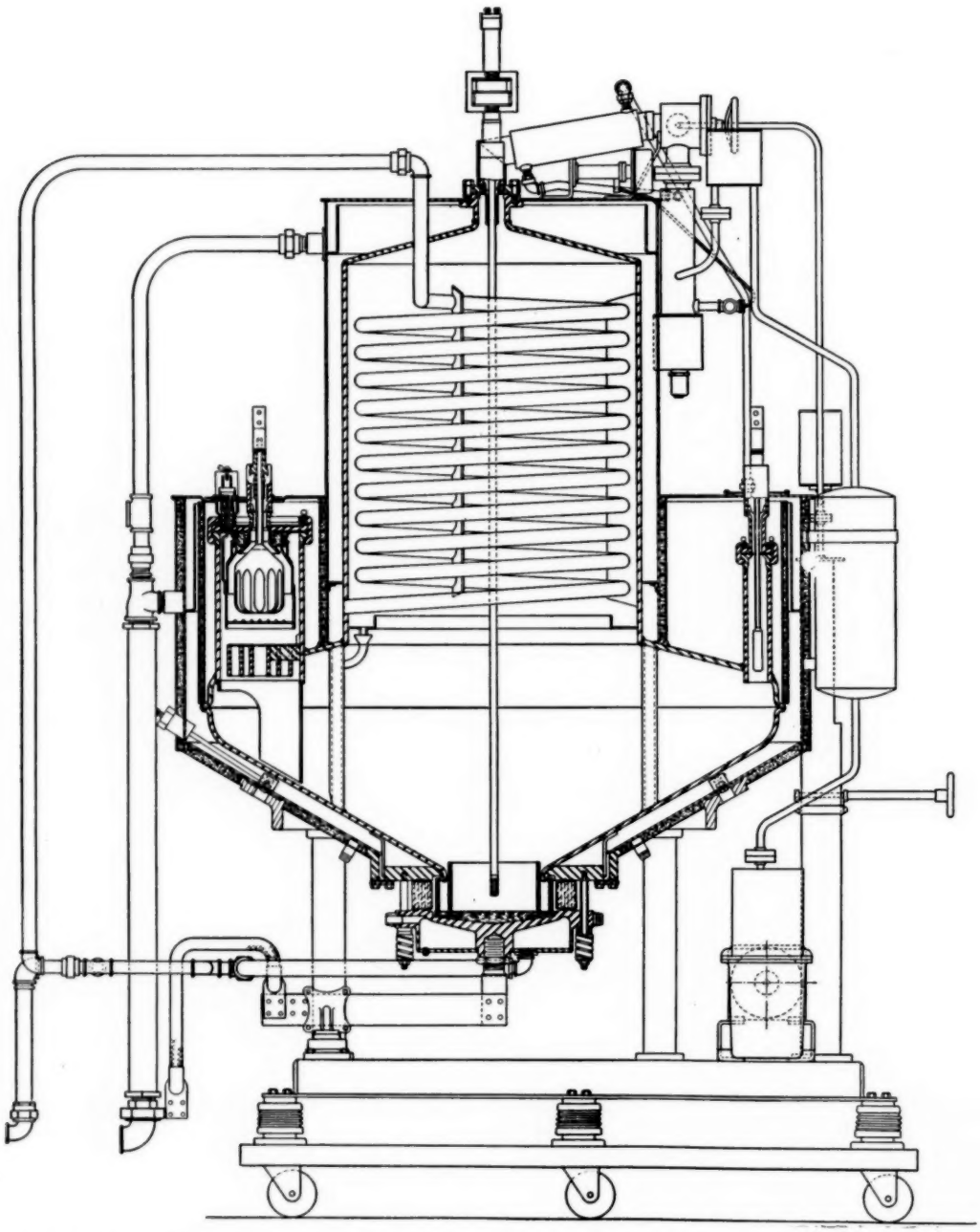

FIG. 2. Mercury-arc type Thyratron. The starting of the current to each anode is controlled by a grid close to the anode.

which is consistent with the above energy calculations. In the FG-98 Thyratron, which is a small filament-type tube containing argon, the grid current required for starting is even smaller, *viz.* 0.002 microampere over its operating range of 50 to 220 volts, as shown in Fig. 7. Its power amplification has approximately the same value, 10^{11}, as the FG-95. With larger tubes, it is probable that an amplification of 10 times this value, *viz.* 10^{12}, could be obtained if desired. For many purposes this high amplification is not needed, and "hard starting" is considered by some to be an advantage in power circuits; so that power Thyratrons are generally

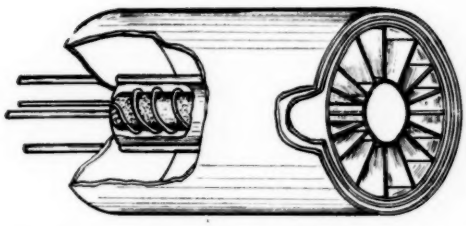

FIG. 3. Cellular type cathode. 250 sq. cm of electron emitting surface are enclosed in a heat shielded cavity with a hole at one end for the escape of electrons. The shielding reduces the heating energy from 1500 watts to 60 watts.

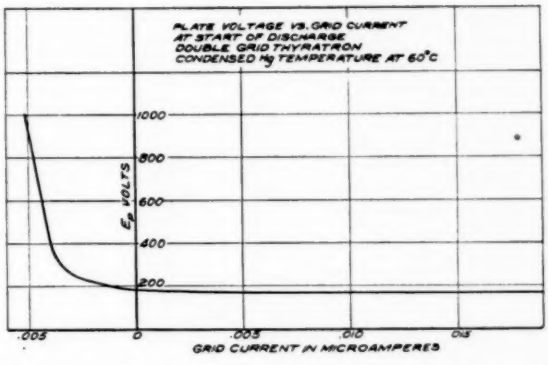

FIG. 5. The grid current required at instant of starting in FG-95 Thyratron, rated at 2.5 amperes, 200–1000 volts.

designed, at present, with a power amplification of about 10^6.

A second important property of the Thyratron is its high efficiency. The first efficiency factor, cathode efficiency, has already been discussed. It may be expressed in terms of the *power cost of electrons*. This, for large cathodes, is approximately 1/2 watt per ampere of emission. In practical circuits, however, the current flows for only 1/2 to 1/12 of the time, so that the average cost, or heating power per used ampere, is from 1 to 6 watts.

The second efficiency factor is the voltage drop in the arc. A typical arc-drop characteristic (Fig. 8) consists of 3 stages: First, a short portion, at approximately the ionization potential, for small currents. Second, a "negative resistance" transition portion, in which the voltage drop falls from the ionizing potential to about the first radiating potential. This occurs when the concentration of metastable atoms becomes sufficient, so that the ions needed can be produced by a two-stage process, namely excitation by 4.9 volt electrons and subsequent raising to the ionization level by impact from 5.4 volt electrons. Third, a long positive re-

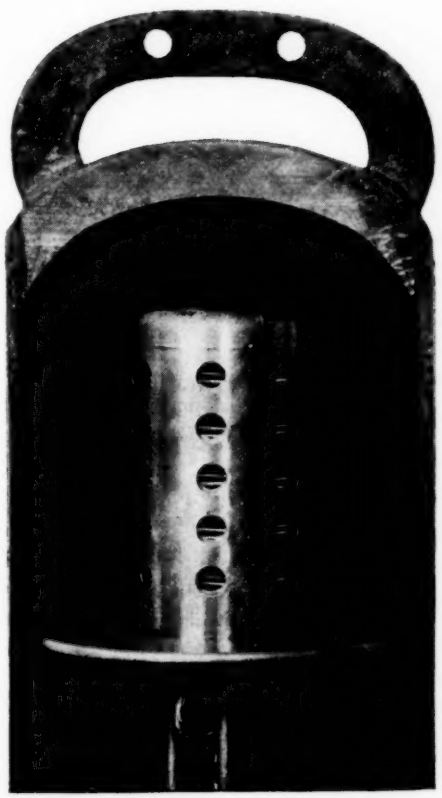

FIG. 4. Alternative type of cellular cathode. The electrons escape through a number of small holes.

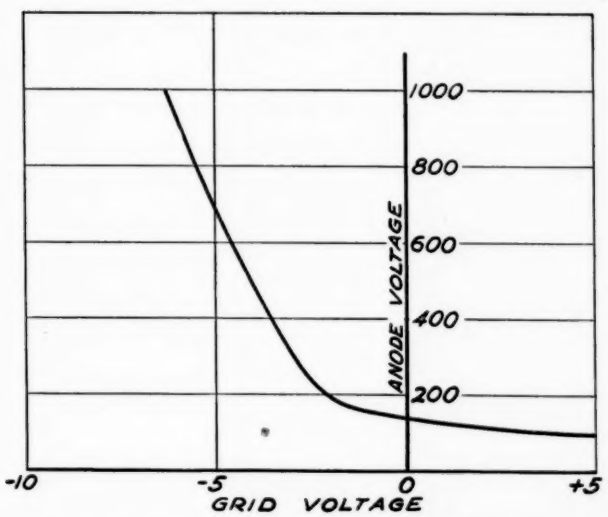

FIG. 6. Control characteristic of FG-95 Thyratron. The control ratio is approximately 1/200.

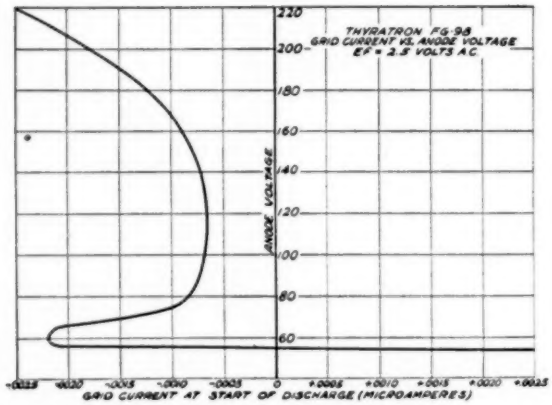

FIG. 7. The grid current at instant of starting in FG-98 Thyratron, rated at ½ ampere, 60–180 volts.

sistance portion, representing the increasing cost of producing positive ions when their number becomes a considerable fraction of the total number of atoms present. This part of the characteristic is a true positive resistance, as proven by the fact that two anodes connected in parallel will share the current equally, for large currents, under all circuit conditions.[3] Practical tube characteristics show the first two portions in varying degree, according to geometry and vapor pressure; but the positive resistance portion is always present, if the tube is fully loaded. This is well illustrated in Fig. 9, which shows the characteristics of the FG-52 Phanotron** at different vapor pressures. The negative resistance

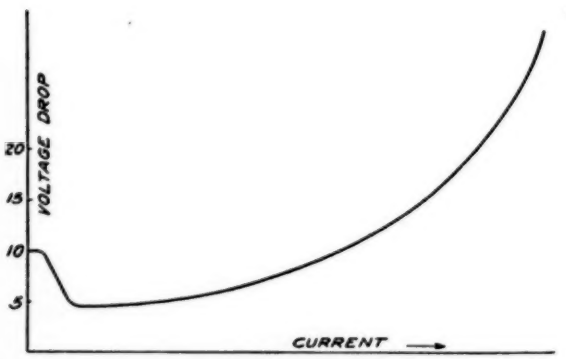

FIG. 8. Typical volt-ampere characteristic of mercury vapor Phanotron. It consists of a short negative resistance portion and a long positive resistance portion.

[3] A. W. Hull and H. D. Brown, *Mercury-Arc Rectifier Research*, Trans. A.I.E.E. **50**, 744–56 (1931).

** The general name *Phanotron* (Greek φαίνω, appear, or be visible) has been given to tubes which combine a thermionic cathode with low-pressure inert gas.

portion, which occurs at currents below 5 amperes, is too short to show on this scale.

From these data it is seen that the sum of the cathode and arc losses is about 7 watts per ampere for a mercury vapor tube with thermionic cathode** under the most favorable conditions. It is 3 watts per ampere for a similar tube with caesium vapor. The corresponding minimum value for a mercury-arc rectifier, or Thyratron with mercury pool cathode, is 20

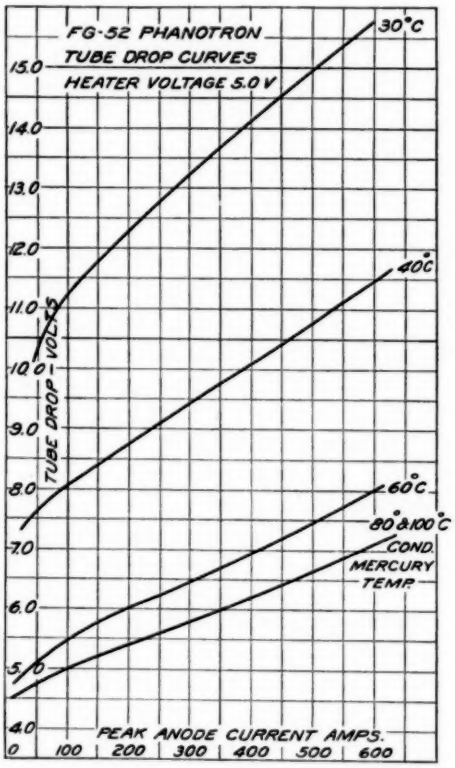

FIG. 9. Volt-ampere characteristics of FG-52 Phanotron at different temperatures. The negative resistance portion of the characteristics is too short to show.

watts per ampere, with the possibility of ultimate reduction to 12, and still lower if caesium is used in place of mercury. Under the most unfavorable conditions, namely high tube-drop and short conducting period in each cycle, the power consumption in the tube is between 25 and 30 watts per ampere at full load, for either the thermionic or pool type.

With these values of tube loss, it is possible to choose circuit and tube conditions so that the tube efficiency lies between 95 and 99 percent, at all practical voltages.

Current and Voltage Limitations

The *current capacity* of the Thyratron is limited only by physical size, since the positive-resistance volt-ampere characteristic, discussed above, insures proper division of current between the parts of a given tube, however large, or between any number of tubes in parallel. At light load, the current is concentrated in a small part of the tube. But as soon as that part attains its normal current, other parts begin to contribute, until all share equally at full load. The maximum present rating of 12-anode mercury-arc Thyratrons is 5000 amperes continuous and 15,000 amperes for short periods. Hot-cathode Thyratrons are available with continuous current rating of 100 amperes; and there appears to be no difficulty in increasing the capacity to 10 or even 100 times this value.

The *voltage* at which Thyratrons can be operated is comparable with that of high vacuum tubes, and the limiting value is probably the same for both, namely the voltage at which autoelectronic emission takes place, independently of gas, due to strong electric fields. The highest rated voltage of present commercial Thyratrons is 15,000 volts, which is about the same as for commercial Pliotrons. But experimental Thyratrons, made by Dr. K. H. Kingdon, have been operated in the laboratory for long periods at 150,000 volts, and for short periods at 200,000 volts.

Time Lag of Ionization and Deionization

The well-known time lag in the starting of a spark discharge in low-pressure gases is due to two factors: *viz.*, the ionization of the gas path, and the building up of cathode emission. In the Thyratron the cathode emission is ready at hand, and only the space-ionization needs to be built up; hence we may expect the time to be much shorter. Fig. 10 shows a cathode-ray oscillogram of the starting time of an FG-57 Thyratron. The upper horizontal curve shows the form of voltage wave used, the lower curve the result of applying this voltage to the anode. The rise in the curve shows the time of application of anode voltage, and its fall, the attainment of full conduction. The sine curve is a timing wave. It will be seen that the *total starting time*, i.e., the interval between the time when the grid becomes positive and the time at which the anode current attains full value, is approximately 2 microseconds. This time is of importance for many scientific applications, such as the timing of stroboscopes and cathode-ray oscillographs, the measurement of instantaneous currents, and the counting of electric impulses.

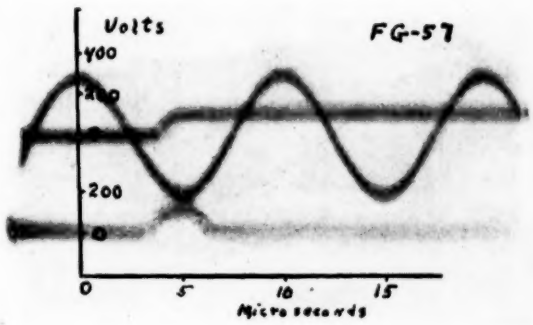

Fig. 10. Time required for starting of FG-57 Thyratron. The two horizontal curves represent voltage between anode and cathode, the upper being the voltage wave without the anode connected, the lower with the anode connected. The application of anode voltage is indicated by the rise in the curve and attainment of full current by its fall. The sine curve is a timing wave.

Deionization, or diffusion of ions to the walls after the current stops, requires a much longer time. It varies from 10 to 500 microseconds according to geometry and vapor pressure. This is the time that must elapse before the grid can again gain control. Fig. 11 shows the positive ion current to the grid of an FG-33 Thyratron, as measured by a cathode-ray oscillograph, immediately after stopping the anode current, for four values of anode current. The decay curve consists of two exponential portions, the first, of about 2 microseconds duration, representing the building of a positive-ion sheath around the grid, the second the diffusion of ions into this sheath.

Methods of Operation

On and off operation

The simplest use of a Thyratron is as a switch, to turn current on and off. It has four properties that recommend it in preference to an ordinary switch or contactor, *viz.*: sensitiveness, or smallness of power needed to control its operation; speed; absence of wear; quietness.

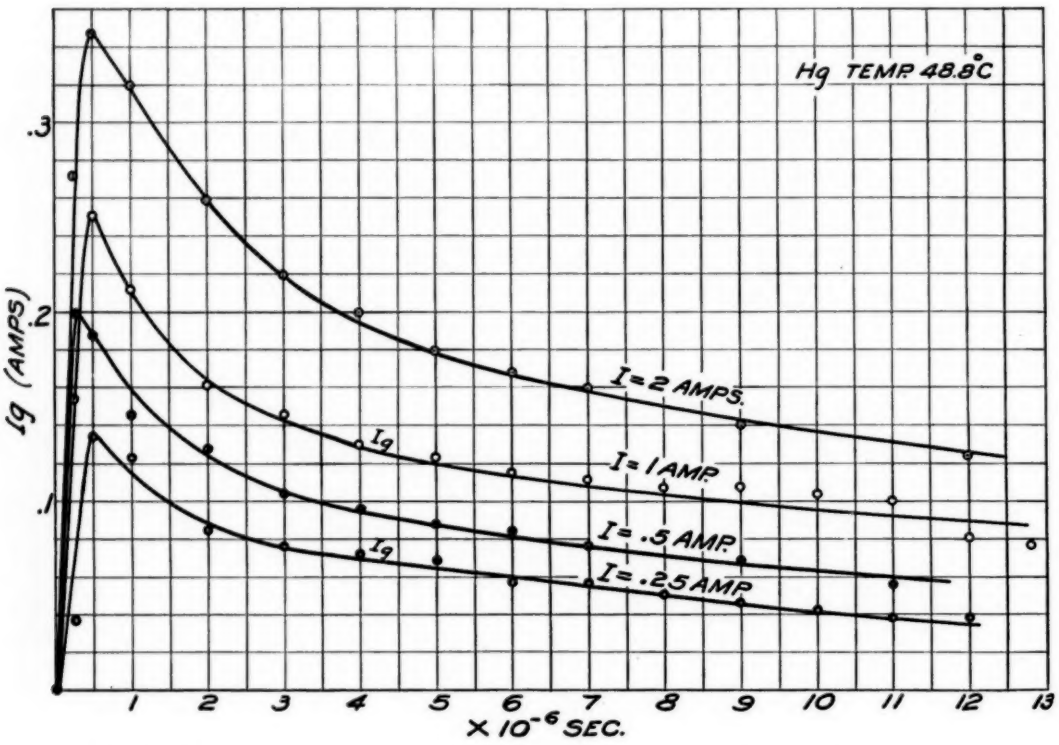

FIG. 11. Grid current after "stopping" in FG-33 Thyratron for 4 values of tube current.

Fig. 12 shows the fundamental circuit for this type of service, when a.c. power is available. The load may be in either the a.c. or the d.c. branch, as indicated, and the controlling element

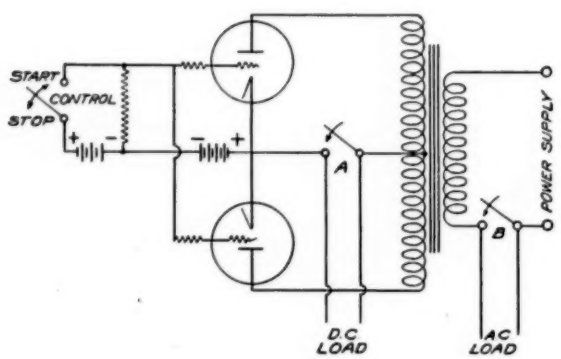

FIG. 12. Typical circuit for using Thyratron as a switch with a.c. power. Note that the load may be placed in either the d.c. (rectified) or a.c. circuit.

may be a manually operated switch, a clock, a thermostat, or a photoelectric tube. The control voltage, E_g, is shown as d.c., but a.c. is equally good and is more often used. The bias voltage E_c is generally a.c. rectified by copper oxide.

When the direct-current output is used, it may be employed to control motors, magnets, or contactors, or to saturate the d.c. windings of reactors in a.c. power circuits, and so control the current in these circuits. This type of operation has found many applications in industrial control,[4] such as turning on lamps at dusk, dispatching products to predetermined stations, cutting hot steel bars to exact length, opening doors at the approach of a person, wrapping packages, sorting beans and other articles, counting people or products.

The load may be placed in the a.c. circuit instead of the d.c. circuit, after closing switch *A* and opening switch *B* in Fig. 12. In this case, when the Thyratrons are not conducting, the transformer *T* constitutes a high impedance in the a.c. circuit; when the Thyratrons are conducting, they short-circuit the secondary of the transformer and make its impedance very low. This type of operation has found application in resistance welding, where its high speed and

[4] W. R. King, *Electron Tubes in Industry*, Trans. A.I.E.E., June, 1931; Chem. and Met. Eng., June, 1932.

exact timing produce results hitherto unattainable.

Fig. 13 shows a method of operating a Thyratron switch with d.c. power supply. The input circuit and method of control is the same as with a.c., but in this case one Thyratron is

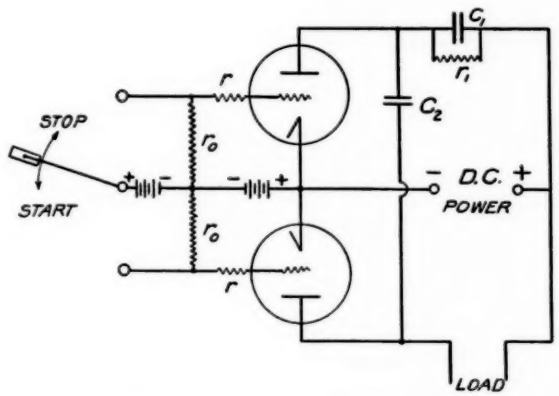

FIG. 13. Typical circuit for operating a Thyratron as a switch, with d.c. power.

started to energize the circuit, the other to de-energize it. The second Thyratron carries only a transient current, which interrupts, momentarily, the current in the first, and thus allows its grid to gain control.

Phase control

There is a still more elegant method of controlling Thyratrons, for which we are indebted to a French engineer, P. Toulon.[5] It consists in varying the phase of the alternating voltage applied to the grid. This varies the time, in each cycle of anode voltage, at which the grid voltage becomes positive, thus "starting" the Thyratron. In the circuit of Fig. 12, if the grids are made positive at the beginning of each cycle the current will be practically continuous; but if they are made positive late in each cycle the current will flow only part of the time, *viz.*, the remaining part of each cycle, and the average current will be less than in the first case. In this way one may obtain any value of *average* current, from maximum value to zero, by smooth continuous steps. It is to be noted that this method of controlling the magnitude of average current, by varying the *fraction of the time* during which current flows, is consistent with high efficiency. The above description applies to a resistance load. With an inductive load the current pulses will be lengthened and may overlap to give a continuous current, but the average value of this current will still depend on the time of starting in each cycle.

An interesting application of this method of Thyratron operation is the dimming and blending of lights in theaters and public buildings.

Rectification

An important application of Thyratrons is *controlled rectification*. All practical generators of electric power generate alternating current, which must be rectified in order to give direct current. Thyratrons are superior to commutators, for this purpose, not only in their freedom from arcing and wear, but in their ability to control the magnitude of the current, thus functioning as voltage regulator, load limiter, and circuit-breaker, as well as switch and commutator; with the additional feature that commutation need not be performed at the generator, but can be applied at any point of the alternating-current network. It is believed that Thyratron rectifiers, thus used, have an important application to the problem of feeding power from the a.c. to the d.c. systems in large cities.

Inversion

The most fascinating application of Thyratrons is changing direct current into alternating. This operation is simply the inverse of rectification, and any good Thyratron rectifier can be operated in either direction by properly controlling the grids. Thus a transformer for alternating current can be converted into a direct-current transformer by the addition of Thyratrons. It is possible that electric power will be transmitted in the future as direct current, especially in cables, on long distance lines, or near telephone wires; or in large systems, where synchronization of alternating machines is difficult. But such large-scale applications must await thorough proving of apparatus and methods, and the working out of many details. One of these details is the effect of the load on

[5] P. Toulon, U. S. Patent 1,289,823; L. Dunoyer and P. Toulon, Comptes Rendus, p. 179, 1924; J. de Physique 257–68, 289–303 (1924).

the inverter. Fig. 14 shows an inverter developed by C. H. Willis,[6] which is capable of supplying alternating current to a load of any power factor, either lagging or leading.

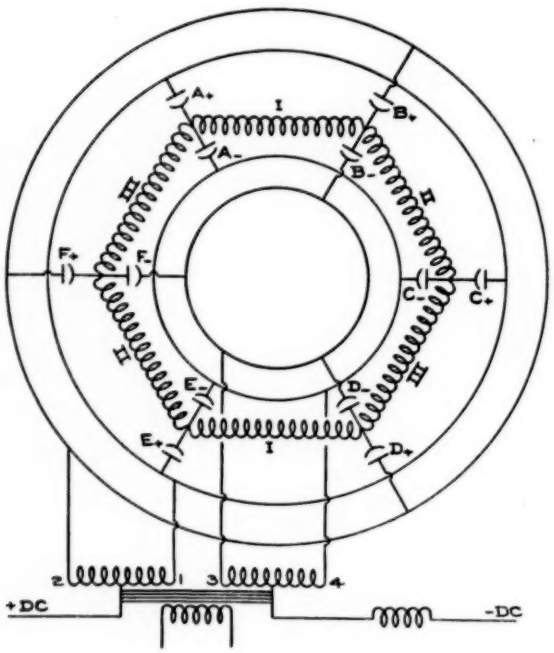

FIG. 14. Inverter circuit with harmonic commutation. Commutating voltage is introduced by the transformer shown at the bottom of the diagram. (C. H. Willis).

Frequency changing

Frequency changing from a higher to a lower frequency is a special case of rectification, in which the Thyratron grids allow current to flow for a number of cycles first in one direction, and then in the other. Similarly, changing from lower to higher frequency is simply inversion, in which the power is drawn alternately from the three phases of the lower frequency. Examples of the first type are the change from 60 to 25 cycles for railway and other power purposes; of the second type the change from 60 to 180 for spinning mills.

Commutation of motors

The commutation of motors, like generators, can be performed much more perfectly by Thyratrons than by brushes. A special advantage of Thyratron commutation is speed control. Fig. 15 shows a synchronous type motor with Thyratron commutators,[7] capable of operating at any speed from zero up to synchronism.

Scientific Applications

The smallest application of Thyratrons, in physical size, may become the greatest if it should lead to an important discovery. This is their use for scientific investigation. Applications of this kind are just beginning, but they include a stroboscope[8] faster than any hitherto devised; a linear timer[9] for the cathode-ray oscillograph; a synchronous switch[10] for interrupting filament heating current while measurements are being made; thermostats; voltage regulators; and circuits for measuring short time intervals,[11] currents of short duration, and end-points in chemical reactions.

The most interesting scientific application is the counting of protons and other products of nuclear disintegration or cosmic radiation. Thus de Bruyne and Webster,[12] and Sparks and Picker-

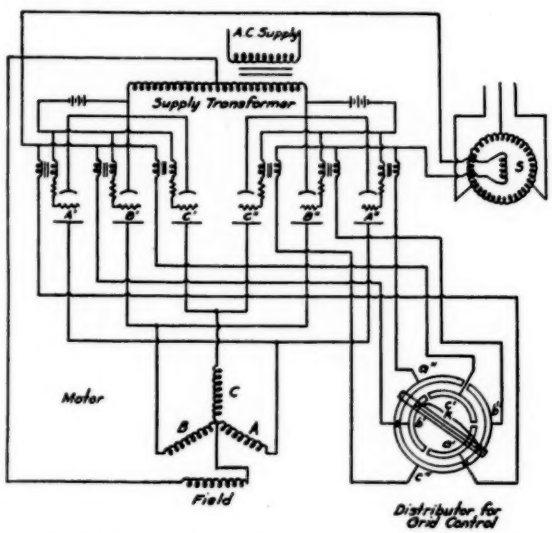

FIG. 15. Variable speed synchronous motor with Thyratrons as commutators. (C. H. Willis).

[6] C. H. Willis, *Harmonic Commutation Using Thyratron Tubes*, Gen. Elec. Rev. **35**, 632–8 (1932) A.I.E.E. paper read January 24, 1933.

[7] C. H. Willis, *The Thyratron-Commutor Motor*, Gen. Elec. Rev. **36**, February, 1933.

[8] H. E. Edgerton, *Stroboscope Using Thyratron Tubes* (to be published soon).

[9] A. L. Samuel, Rev. Sci. Inst. **2**, 532 (1931).

[10] W. B. Nottingham, Phys. Rev. **37**, 1690A (1931).

[11] K. J. Sixtus and L. Tonks, Phys. Rev. **37**, 930 (1931).

[12] N. A. de Bruyne and H. C. Webster, Proc. Camb. Phil. Soc. **27**, 113 (1931).

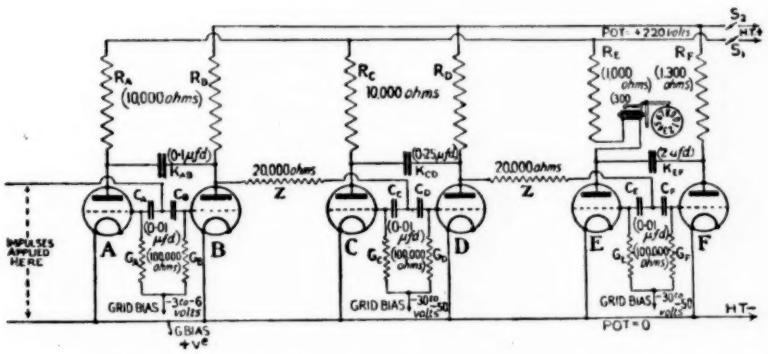

FIG. 16. "Scale of Two" Thyratron Counter, by C. E. Wynn-Williams.

ing[13] have applied the Thyratron to the recording of coincidences of two or more Geiger counters. Rutherford and Wynn-Williams[14] have used the combination of vacuum tube amplifier and Thyratron to count alpha-particles, making possible the separation of particles of different range, or different ionizing power at any part of their range, to a degree hitherto unattainable. Most important of all, Wynn-Williams[15] has devised a method (Fig. 16) of high-speed counting by means of Thyratrons, which appears capable of counting, infallibly, any number of particles, at a speed limited only by the deionization time of the Thyratrons. This time may be made less than 10 microseconds, so that it should be possible to register separately particles which arrive 10^{-5} sec. apart, and perhaps as close as 10^{-6} sec. apart.

These methods, with better Pliotron amplifiers, of which the PJ-11[16] is a first example, and faster Thyratrons, of which the FP-95 is a forerunner (See characteristics, Figs. 5 and 6) will help to speed the attack on the nucleus, which many laboratories, with million-volt missiles, are preparing to storm.

[13] B. Sparks and W. Pickering, Meeting of American Physical Society, December 17, 1932.

[14] Rutherford, Wynn-Williams and Lewis, Proc. Roy. Soc. **A133**, 351 (1931).

[15] C. E. Wynn-Williams, Proc. Roy. Soc. **A132**, 295–310 (1931); **A136**, 312–24 (1932).

[16] G. F. Metcalf and T. M. Dickinson, Physics **3**, 11–17 (1932).

Mutual Impedance of Long Grounded Wires When the Conductivity of the Earth Varies Exponentially with Depth

MARION C. GRAY, *American Telephone and Telegraph Company*

(Received December 12, 1932)

This paper presents a formula for the mutual impedance of long grounded wires above the surface of the earth, on the assumption that the conductivity of the earth varies exponentially with depth according to the formula $\gamma=\gamma_0 e^{-bz}$. For $b=0$ the formula reduces to the known result for a uniformly conducting earth, while if b is allowed to become negatively infinite it reduces to the result for an earth consisting of a conducting layer at the surface only. For small values of b the first terms in the expansion of the impedance formula in powers of b are obtained, and curves are included of the real and imaginary parts of the coefficient of b.

FORMULAE for the mutual impedance of overhead wires parallel to the surface of the earth have been published with various assumptions as to the conductivity of the earth. Thus Pollaczek[1] and Carson[2] assumed a uniform conductivity, while Mayr[3] assumed a conducting layer at the surface only. In both these cases the conductivity is defined by a single parameter, but Haberland[4] combined the two assumptions to consider the two-parameter case of an earth of uniform conductivity with a thin surface layer of greater conductivity. More recently Evans[5] has generalized the Haberland case by assuming that the upper conducting layer is of finite depth, thus introducing three conductivity parameters. In the present paper we consider another two-parameter case and derive a mutual impedance formula on the assumption that the conductivity of the earth varies exponentially with depth.[6]

We consider an infinite wire of negligible diameter at height h above the surface of the earth (assumed plane), and carrying a current $Ie^{i\omega t}$. As usual the exponential factor is omitted throughout. The surface of the earth is taken as the x–y plane, the wire being parallel to the x axis, and the z axis extends vertically upwards into the air. The frequency, $\omega/(2\pi)$, is assumed to be sufficiently low to allow all displacement currents to be neglected. The inductivities of both earth and air are taken equal to that of free space ν, and their capacitivities zero; the conductivity of the air is also assumed to be zero, while the conductivity of the earth is defined by the formula

$$\gamma=\gamma_0 e^{-bz}, \qquad z\leqq 0, \tag{1}$$

where γ_0 is the conductivity at the surface ($z=0$), and we shall at first assume that the real constant b is positive. All distances are measured in meters, impedances in ohms and conductivities in mhos per meter; ν has the value 1.256×10^{-6} henries per meter.

Since the wire is very long we may neglect the components E_y and E_z of the electric field as compared with E_x, and the differential equations satisfied by E_x and the magnetic components H_y and H_z are therefore,

$$i\omega\nu H_y=-\partial E_x/\partial z, \tag{2}$$

$$i\omega\nu H_z=\partial E_x/\partial y, \tag{3}$$

$$\gamma_0 e^{-bz}E_x=\partial H_z/\partial y-\partial H_y/\partial z, \tag{4}$$

where the electric field is expressed in volts per meter, the magnetic field in ampere-turns per meter. From these equations the differential equation for E_x is easily found to be

$$\partial^2 E_x/\partial y^2+\partial^2 E_x/\partial z^2=\Gamma_0^2 e^{-bz}E_x, \tag{5}$$

[1] F. Pollaczek, Elekt. Nachr. Tech. **3**, 339–359 (1926).
[2] J. R. Carson, Bell Sys. Tech. J. **5**, 539–554 (1926).
[3] O. Mayr, Elektrotech. Zeits. **46**, 1352–1355 (1925).
[4] G. Haberland, Zeits. angew. Math. **6**, 366–379 (1926).
[5] H. P. Evans, Phys. Rev. **36**, 1579–1588 (1930).
[6] A similar assumption has been made recently by G. J. Elias, Elekt. Nachr. Tech. **8**, 4–22 (1931), in connection with a different problem.

where $\Gamma_0=(i\omega\nu\gamma_0)^{1/2}$ is the propagation constant at the earth's surface. A solution of this equation which vanishes at an infinite depth is

$$E_x=\int_0^\infty f(\mu)K_{2\beta\mu}(2\beta\Gamma_0 e^{-bz/2})\cos y\mu\, d\mu, \quad (6)$$

where we have written β for $1/b$. Here $K_\alpha(\zeta)$ is the Bessel function of the second kind with imaginary argument as defined by G. N. Watson,[7] and $f(\mu)$ is an arbitrary function of its argument to be determined by the boundary conditions. These conditions are that E_x and H_y must be continuous at the surface, $z=0$, and from Eq. (2) it follows that the continuity of H_y may be replaced by the continuity of $\partial E_x/\partial z$.

In the air the electric field E_{x0} at the point (y, z) may be formulated as

$$E_{x0}=\frac{i\omega\nu I}{2\pi}\log\frac{[y^2+(h-z)^2]^{1/2}}{[y^2+(h+z)^2]^{1/2}}+\int_0^\infty \phi(\mu)e^{-z\mu}\cos y\mu\, d\mu, \quad (7)$$

where the first term gives the field due to the primary current in the wire,[8] while the second term represents the secondary field, $\phi(\mu)$ being at present arbitrary. From Eqs. (6) and (7) using the two boundary conditions, we have the following equations to determine the two functions $f(\mu)$ and $\phi(\mu)$,

$$K_{2\beta\mu}(2\beta\Gamma_0)f(\mu)=\phi(\mu), \quad (8)$$

$$\Gamma_0 K'_{2\beta\mu}(2\beta\Gamma_0)f(\mu)=(i\omega\nu I/\pi)e^{-h\mu}+\mu\phi(\mu), \quad (9)$$

where in obtaining Eq. (9) we have used the Fourier integral

$$h/(h^2+y^2)=\int_0^\infty e^{-h\mu}\cos y\mu\, d\mu.$$

With the use of the recurrence formulae for the Bessel functions, the solution of these equations is

$$f(\mu)=-\frac{i\omega\nu I}{\pi\Gamma_0}\frac{e^{-h\mu}}{K_{2\beta\mu+1}(2\beta\Gamma_0)}, \quad (10)$$

$$\phi(\mu)=-\frac{i\omega\nu I}{\pi\Gamma_0}\frac{K_{2\beta\mu}(2\beta\Gamma_0)}{K_{2\beta\mu+1}(2\beta\Gamma_0)}e^{-h\mu}. \quad (11)$$

The electric field in the air is therefore determined as

$$E_{x0}=-\frac{i\omega\nu I}{2\pi}\log\frac{[y^2+(h+z)^2]^{1/2}}{[y^2+(h-z)^2]^{1/2}}-\frac{i\omega\nu I}{\pi\Gamma_0}\int_0^\infty\frac{K_{2\beta\mu}(2\beta\Gamma_0)}{K_{2\beta\mu+1}(2\beta\Gamma_0)}e^{-(h+z)\mu}\cos y\mu\, d\mu. \quad (12)$$

The mutual impedance per unit length between two infinite parallel wires at heights h and H above the earth's surface may be written down immediately:

$$Z_{12}=\frac{i\omega\nu}{2\pi}\log\frac{[y^2+(h+H)^2]^{1/2}}{[y^2+(h-H)^2]^{1/2}}+\frac{i\omega\nu}{\pi\Gamma_0}\int_0^\infty\frac{K_{2\beta\mu}(2\beta\Gamma_0)}{K_{2\beta\mu+1}(2\beta\Gamma_0)}e^{-(h+H)\mu}\cos y\mu\, d\mu. \quad (13a)$$

The solution (13a) has been obtained on the assumption that the conductivity of the earth is increasing exponentially with depth ($0<b$). If, however, we wish to include negative values of b, the formula is easily modified, the only change in the derivation being that the solution (6) of Eq. (5) is no longer valid, and must be replaced by the solution

$$E_x=\int_0^\infty f(\mu)I_{-2\beta\mu}(-2\beta\Gamma_0 e^{-bz/2})\cos y\mu\, d\mu, \quad (6')$$

where $I_\alpha(\zeta)$ is the Bessel function of the first kind with imaginary argument as defined by Watson.[9] Then in place of (13a) we find the formula

$$Z_{12}=\frac{i\omega\nu}{2\pi}\log\frac{[y^2+(h+H)^2]^{1/2}}{[y^2+(h-H)^2]^{1/2}}+\frac{i\omega\nu}{\pi\Gamma_0}\int_0^\infty\frac{I_{-2\beta\mu}(-2\beta\Gamma_0)}{I_{-2\beta\mu-1}(-2\beta\Gamma_0)}e^{-(h+H)\mu}\cos y\mu\, d\mu. \quad (13b)$$

[7] G. N. Watson, *Theory of Bessel Functions*, Cambridge, 1922, page 78.

[8] Reference 5, page 1583.

[9] Reference 7, page 77.

If we put $b=0$ both (13a) and (13b) reduce to the well-known formula[10]

$$Z_{12}=\frac{i\omega\nu}{2\pi}\log\frac{[y^2+(h+H)^2]^{1/2}}{[y^2+(h-H)^2]^{1/2}}+\frac{i\omega\nu}{\pi\Gamma_0^2}\int_0^\infty[(\mu^2+\Gamma_0^2)^{1/2}-\mu]e^{-(h+H)\mu}\cos y\mu\,d\mu \tag{14}$$

for a uniformly conducting earth. Further, by allowing β to approach zero through negative values while at the same time γ_0 becomes infinite in such a way that $\gamma_1=-\beta\gamma_0$ remains finite, we obtain

$$Z_{12}=\frac{i\omega\nu}{2\pi}\log\frac{[y^2+(h+H)^2]^{1/2}}{[y^2+(h-H)^2]^{1/2}}+\frac{i\omega\nu}{2\pi}\int_0^\infty\frac{1}{\mu+\frac{1}{2}i\omega\nu\gamma_1}e^{-(h+H)\mu}\cos y\mu\,d\mu, \tag{15}$$

which is Mayr's result[11] for a conducting layer at the surface only.

Returning to Eq. (13a) let us simplify it by making the substitutions $\beta'=\Gamma_0(2i)^{-1/2}\beta$, $y'=\Gamma_0(2i)^{-1/2}y$, with similar definitions of h' and H', thus multiplying all distances by the attenuation constant. We then have

$$Z_{12}=\frac{i\omega\nu}{2\pi}\log\frac{[y'^2+(h'+H')^2]^{1/2}}{[y'^2+(h'-H')^2]^{1/2}}+\frac{i\omega\nu}{\pi(2i)^{1/2}}\int_0^\infty\frac{K_{2\beta'\mu}[2(2i)^{1/2}\beta']}{K_{2\beta'\mu+1}[2(2i)^{1/2}\beta']}e^{-(h'+H')\mu}\cos y'\mu\,d\mu. \tag{13}$$

For the important case of small values of $b'(=1/\beta')$ it is possible to expand Z_{12} in a series of powers of b', the first terms of the expansion being

$$Z_{12}=(\omega\nu/2\pi)\{i\log[y'^2+(h'+H')^2]^{1/2}/[y'^2+(h'-H')^2]^{1/2}+P_0(h'+H',y')$$
$$+b'P_1(h'+H',y')+b'^2P_2(h'+H',y')+\cdots\}, \tag{16}$$

where

$$P_0(h,y)=\int_0^\infty[(\mu^2+2i)^{1/2}-\mu]e^{-h\mu}\cos y\mu\,d\mu, \tag{17}$$

$$P_1(h,y)=\frac{1}{2}\int_0^\infty\left[\frac{\mu}{(\mu^2+2i)^{1/2}}-\frac{\mu^2+i}{\mu^2+2i}\right]e^{-h\mu}\cos y\mu\,d\mu, \tag{18}$$

$$P_2(h,y)=\frac{i}{8}\int_0^\infty\left[\frac{4\mu^2+3i}{(\mu^2+2i)^{5/2}}-\frac{4\mu}{(\mu^2+2i)^2}\right]e^{-h\mu}\cos y\mu\,d\mu. \tag{19}$$

This expansion is valid for either positive or negative values of b'. In Eq. (16) the first term is the mutual impedance for an earth of infinite conductivity, the second term is the Carson correction for a uniform finite conductivity, while the third term gives an approximate correction for an earth whose conductivity increases or decreases slowly with depth.

An expansion of the integral (17) in a form suitable for computation has already been given by Carson[12] in terms of the polar coordinates (r,θ), where $h=r\cos\theta$, $y=r\sin\theta$. A similar, though more complicated, expansion for the integral (18) is as follows:

$$P_1(h,y)\equiv P_1(r,\theta)=U_1(r,\theta)+iV_1(r,\theta)$$

where

$$2U_1(r,\theta)=(\pi/8)[\cos A\cosh B+\cos B\cosh A+\sin A\sinh B+\sin B\sinh A]-S_1-S_2$$
$$+\tfrac{1}{4}\pi(S_4-S_3)+\tfrac{1}{2}(S_5+S_6)\log 2+(S_5-S_6)\log r-\Sigma_5+\Sigma_6+(S_6'-S_5')\theta, \tag{20}$$

[10] Reference 1, formula (23b); reference 2, formula (24); reference 4, formula (18).

[11] Reference 3, formula (13). To obtain Mayr's formula we have to put $h=0$ in Eq. (15).

[12] Reference 2, formulae (32) and (33).

$$2V_1(r,\theta)=(\pi/8)[\cos A\cosh B+\cos B\cosh A-\sin A\sinh B-\sin B\sinh A]-S_1+S_2$$
$$+\tfrac{1}{2}(S_3+S_4)\log 2+(S_3-S_4)\log r-\Sigma_3+\Sigma_4+(S_4'-S_3')\theta+\tfrac{1}{4}\pi(S_5-S_6). \quad (21)$$

In these expansions we have written $A=r(\cos\theta+\sin\theta)$, $B=r(\cos\theta-\sin\theta)$, and the convergent series are defined as follows,

$$S_1=1-\frac{2^2r^4\cos 4\theta}{3^2\cdot 5}+\frac{2^4r^8\cos 8\theta}{3^2\cdot 5^2\cdot 7^2\cdot 9}-\cdots,$$

$$S_2=\frac{2r^2\cos 2\theta}{3}-\frac{2^3r^6\cos 6\theta}{3^2\cdot 5^2\cdot 7}+\frac{2^5r^{10}\cos 10\theta}{3^2\cdot 5^2\cdot 7^2\cdot 9^2\cdot 11}-\cdots,$$

$$S_3=r\cos\theta-\frac{2^2r^5\cos 5\theta}{5!}+\frac{2^4r^9\cos 9\theta}{9!}-\cdots,$$

$$\Sigma_3=r\cos\theta\,\psi(2)-\frac{2^2r^5\cos 5\theta}{5!}\psi(6)+\frac{2^4r^9\cos 9\theta}{9!}\psi(10)-\cdots,$$

$$S_4=r\cos\theta-\frac{r^5\cos 5\theta}{2^2 2!\,3!}+\frac{r^9\cos 9\theta}{2^4 4!\,5!}-\cdots,$$

$$\Sigma_4=r\cos\theta\left[\psi(1)+\frac{1}{2}\right]-\frac{r^5\cos 5\theta}{2^2 2!\,3!}\left[\psi(3)+\frac{1}{6}\right]+\frac{r^9\cos 9\theta}{2^4 4!\,5!}\left[\psi(5)+\frac{1}{10}\right]-\cdots,$$

$$S_5=\frac{2r^3\cos 3\theta}{3!}-\frac{2^3r^7\cos 7\theta}{7!}+\frac{2^5r^{11}\cos 11\theta}{11!}-\cdots,$$

$$\Sigma_5=\frac{2r^3\cos 3\theta}{3!}\psi(4)-\frac{2^3r^7\cos 7\theta}{7!}\psi(8)+\frac{2^5r^{11}\cos 11\theta}{11!}\psi(12)-\cdots,$$

$$S_6=\frac{r^3\cos 3\theta}{2\cdot 1!\,2!}-\frac{r^7\cos 7\theta}{2^3 3!\,4!}+\frac{r^{11}\cos 11\theta}{2^5 5!\,6!}-\cdots,$$

$$\Sigma_6=\frac{r^3\cos 3\theta}{2\cdot 1!\,2!}\left[\psi(2)+\frac{1}{4}\right]-\frac{r^7\cos 7\theta}{2^3 3!\,4!}\left[\psi(4)+\frac{1}{8}\right]+\frac{r^{11}\cos 11\theta}{2^5 5!\,6!}\left[\psi(6)+\frac{1}{12}\right]-\cdots,$$

and $S_n'(r,\theta)=S_n(r,\tfrac{1}{2}\pi-\theta)$, $n=3,\ 4,\ 5,\ 6$.

The function $\psi(n)$ appearing in the Σ series is the logarithmic derivate of the gamma-function.[13]

From these expansions curves have been drawn showing the real and imaginary parts of $P_1(r,\theta)$ as a function of r for values of $\cos\theta=0,\ \frac{1}{4},\ \frac{1}{2},\ \frac{3}{4},\ 1$. Figs. 1 to 4. Equal intervals of $\cos\theta$ were used rather than equal intervals of θ itself, since it was found that this procedure gave a much more evenly spaced set of curves. For convenience of reference, curves for the real and imaginary parts of $P_0(r,\theta)$ are also given, these being obtained from Carson's expansions with slight alterations due to changes of notation.[14] It may be worth while to note that for wires on the surface of

[13] See e.g., E. T. Whittaker and G. N. Watson, *Modern Analysis*, Third Edition, Cambridge, 1920, page 241. When n is an integer $\psi(n+1)=-\gamma+1+\frac{1}{2}+\frac{1}{3}+\cdots+(1/n)$, where γ is Euler's constant and has the value 0.57722.

[14] In drawing the curves for $\cos\theta=1$ and $\cos\theta=\frac{1}{2}$, use was made of the tables of values published by J. E. Clem, Trans. Amer. Inst. Elect. Eng. **50**, 909–910 (1931).

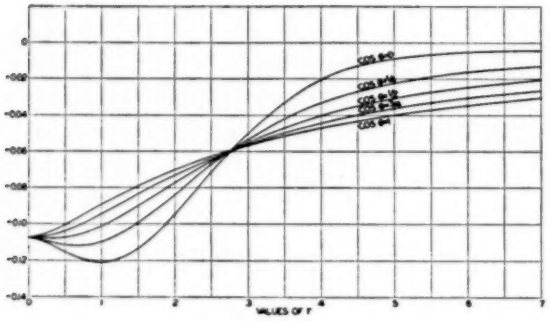

FIG. 1. $U_1(r, \theta)$ = Real part of $P_1(r, \theta)$.

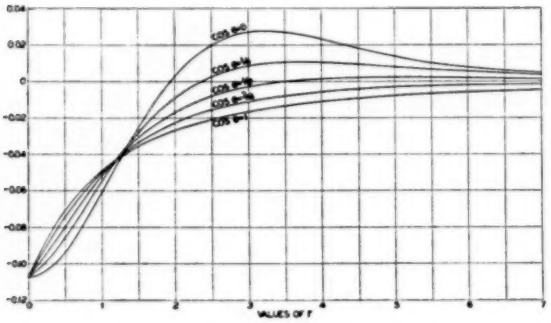

FIG. 2. $V_1(r, \theta)$ = Imaginary part of $P_1(r, \theta)$.

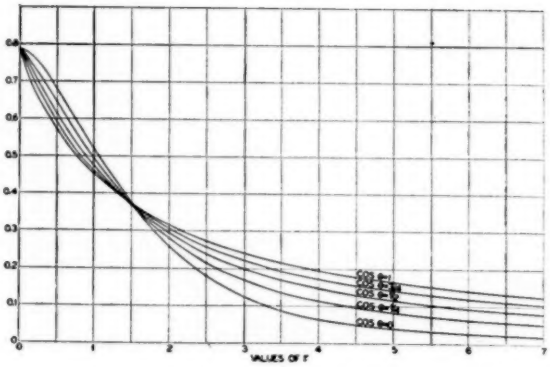

FIG. 3. $U_0(r, \theta)$ = Real part of $P_0(r, \theta)$.

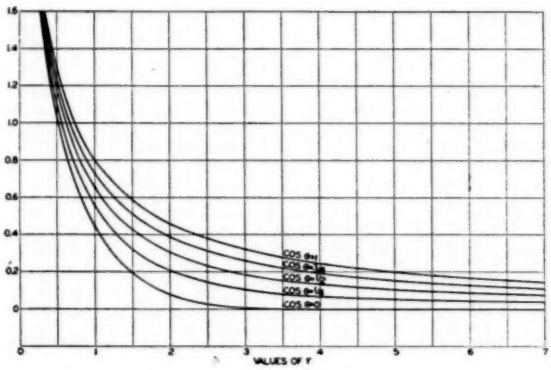

FIG. 4. $V_0(r, \theta)$ = Imaginary part of $P_0(r, \theta)$.

the earth ($\theta = \pi/2$), the expansions (20) and (21) take the much simpler form

$$2U_1 = \tfrac{1}{4}\pi e^{-y}(\cos y + \sin y) + 2^{-1/2}\pi \mathrm{ber}'(2^{1/2}y) - S_1(y, 0) + S_2(y, 0),$$

$$2V_1 = \tfrac{1}{4}\pi e^{-y}(\cos y - \sin y) + 2^{-1/2}\pi \mathrm{bei}'(2^{1/2}y) - S_1(y, 0) - S_2(y, 0),$$

where $\mathrm{ber}'(z)$, $\mathrm{bei}'(z)$ are derivatives of the Bessel functions of the first kind and of complex argument.[15]

Finally for large values of r an approximation to the value of $P_1(r, \theta)$ is given by the asymptotic expansion

$$P_1(r, \theta) = -\frac{\cos\theta}{4r} + \frac{\cos 2\theta}{4r^2} + \frac{3\cos 4\theta}{8r^4} - \frac{3\cos 5\theta}{2r^5} + \cdots + i\left[-\frac{\cos 2\theta}{4r^2} + \frac{\cos 3\theta}{4r^3} + \frac{3\cos 4\theta}{8r^4} + \cdots\right].$$

In conclusion I wish to record my gratitude to Mr. R. M. Foster for many helpful suggestions in the course of this work.

[15] Tables of values of these functions have been published by H. B. Dwight, Trans. Amer. Inst. Elect. Eng. **48**, 812 (1929).

Capacitance and Potential Gradients of Eccentric Cylindrical Condensers

CHESTER L. DAWES, *The Harvard Engineering School*

(Received November 7, 1932)

SOMETIMES it becomes desirable to calculate the capacitance and the potential gradient of eccentric cylindrical condensers, for example, with cables and with special condensers. Although methods have been evolved which give the capacitance and potential gradient in such condensers *,[1,2] very little literature giving a complete but compact treatment of the subject is available. Moreover, the different formulas presented here are derived on a somewhat different basis than is ordinarily adopted. Several forms of the same formula together with their analysis are presented. The formulas are derived from the well-known method of inverse points and images.[3] For simplicity, the formulas are derived in statfarads per cm length, with vacuum as the dielectric ($\kappa=1$). It is a simple matter to apply the necessary coefficients for the desired lengths and for other dielectrics.

Fig. 1 shows the cross section of the two eccentric cylinders, both of which are very thin; the radius of the outer cylinder is b cm and its center is at C'; the radius of the inner cylinder is a cm and its center is at C. The distance between C' and C is c cm. Let P be any point on the surface of the inner cylinder; draw CP.

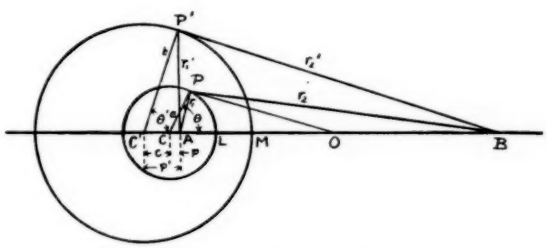

FIG. 1. Eccentric cylinders and inverse points.

Also draw the straight line BCC' and locate points A and B such that

$$CA \times BC = a^2 \tag{1}$$

and

$$C'A \times BC' = b^2. \tag{2}$$

The charge on the inner cylinder is $+Q$ e.s.u. per cm length and the charge on the outer cylinder is $-Q$ e.s.u. per cm length. Let the potential of the inner cylinder be V_1 statvolts above earth potential and the potential of the outer cylinder V_2 statvolts above earth potential.

A and B are the inverse points of the system. So far as the outer cylinder is concerned the effect of the charge on the inner cylinder is as if the charge $+Q$ were concentrated uniformly along the axis corresponding to the point A; so far as the inner cylinder is concerned the effect of the charge on the outer cylinder is as if the charge $-Q$ were concentrated uniformly along the axis corresponding to the point B. This may be demonstrated as follows:

Let O, the midpoint between A and B, be at zero or earth potential. Draw OP; $AP=r_1$; and $BP=r_2$. The potential at P, or the work done in carrying a unit charge from O to P against the forces due to $+Q$ at A and $-Q$ at B, is

$$W = V_p = V_1 = \int_{r_1}^{OA} \frac{2Q}{r}\,dr + \int_{OB}^{r_2} \frac{2Q}{r}\,dr$$
$$= 2Q \log_e r_2/r_1 \tag{3}$$

where $\log_e$ is the logarithm to the Napierian base.

In triangles CPA and CPB the angle θ is common from (1), $CA/CP = CP/BC$; they are, therefore, similar.

It also follows that

$$BP/AP = r_2/r_1 = BC/CP. \tag{4}$$

Maintain r_2/r_1 constant so that V_p remains constant.

* Reference 3, pp. 168–170.

[1] Mayo D. Hersey, *The Resistance, Inductance and Capacity of Eccentric Cylinders.* Elec. World **56**, 435 (1910).

[2] Alexander Russell, *Problems in Connection with the Electrified Cylindrical Conductors.* J. Inst. Elec. Eng. **64**, 238 (1925–26).

[3] Alexander Russell, *A Treatise on the Theory of Alternating Currents.* Cambridge University Press (1914).

It is well known that, if a point so moves that the ratio of its distances from two fixed points is constant, its locus is a circle. Hence the locus of P is a circle, since from (1) and (4) CP or its radius a is constant. From Green's theorem, the presence of the cylinder with a as its radius does not change the potential relations due to the charge along the axis corresponding to the point A, at points external to the inner cylinder.

Let P' be a point on the inner surface of the outer cylinder; draw $C'P'$, AP' and BP' where $AP'=r_1'$ and $BP'=r_2'$. Triangles $BC'P'$ and $AC'P'$ have the angle θ' in common and from (2), $C'A/C'P'=C'P'/BC'$; these triangles are, therefore, similar and

$$BP'/AP'=r_2'/r_1'=BC'/C'P'. \qquad (5)$$

If r_2'/r_1' is maintained constant, the locus of P' is also a circle with C' as a center and b as a radius. In a manner similar to that used to determine the potential of point P (3), it may be shown that the potential of P',

$$V_{p'}=V_2=2Q\log_e(r_2'/r_1'). \qquad (6)$$

By Green's theorem the presence of the outer cylinder does not disturb the potential relations in the field due to the charges at A and B. Therefore, so far as the inner cylinder is concerned, the charge on the outer cylinder acts as if it were concentrated along the axis corresponding to the point B.

Let L and M be the intersections of the line AB with the inner and outer cylinders respectively; let the distance $CA=p$ and the distance $C'A=p'$.

When point P coincides with L and point P' with M, from (4) and (5),

$$BL/AL=r_2/r_1=BC/a;\ BM/AM=r_2'/r_1'=BC'/b.$$

From (3) and (6),

$$V_1=2Q\log_e(BC/a); \qquad V_2=2Q\log_e(BC'/b)$$
$$V_1-V_2=2Q\log_e(b/a)\times(BC/BC').$$

From (1) and (2),

$$BC=a^2/CA=a^2/p; \qquad BC'=b^2/C'A=b^2/p'.$$

Hence,

$$V_1-V_2=2Q\log_e((b/a)(a^2p'/b^2p))$$

and the capacitance

$$C=Q/(V_1-V_2)=1/[2\log_e((b/a)(a^2p'/b^2p))]. \qquad (7)$$

Before the capacitance can be found, p and p' must be determined.

$$BC=a^2/p; \qquad BC'=b^2/p'$$
$$BC'-BC=c \qquad \therefore\ b^2/p'-a^2/p=c \qquad (I)$$
$$c=p'-p. \qquad (II)$$

Solving (I) and (II) simultaneously,

$$p=m/2c\pm[(m/2c)^2-a^2]^{1/2}, \qquad (8)$$
$$p'=m'/2c\pm[(m'/2c)^2-b^2]^{1/2}, \qquad (9)$$

where $m=b^2-a^2-c^2$ and $m'=b^2-a^2+c^2$.

When the minus signs in (8) and (9) are used, the values of p and p' are equal to CA and $C'A$. If the positive signs are used, the values of p and p' are equal to CB and $C'B$, that is the distances from C and C' to the other inverse point B. The correct result is obtained with either sign; with the positive signs, the value of capacitance becomes negative, corresponding to a direction of work which is negative to that assumed in deriving (3) and (6).

The capacitance may be determined by substituting the values of p and p' of (8) and (9) in (7).

The capacitance may be expressed in four quite different forms. The form which may be used is determined by whether it is convenient to use logarithmic functions or hyperbolic functions or whether it is desired to make comparison with the capacitance of a concentric cylindrical condenser in which the cylinders have the same radii as for the eccentric case.

(a) By substituting (8) and (9) directly in (7),

$$C=\frac{Q}{V_1-V_2}=\left\{2\log_e\left[\frac{a}{b}\times\frac{m'-(m'^2-4b^2c^2)^{1/2}}{m-(m^2-4a^2c^2)^{1/2}}\right]\right\}^{-1}. \qquad (10)$$

This formula involves logarithmic functions only. Positive signs before the radical may be used as well as negative signs.

(b) The substitution of (8) and (9) in (7) may be made as follows:

$$C=\left\{2\log_e\frac{b}{a}+2\left[2\log_e\frac{a}{b}+\log_e\frac{m'-(m'^2-4b^2c^2)^{1/2}}{m-(m^2-4a^2c^2)^{1/2}}\right]\right\}^{-1} \tag{11}$$

$$=\left\{2\left[\log_e\frac{b}{a}+\log_e\left(\left(\frac{a}{b}\right)^2\times\frac{m'-(m'^2-4b^2c^2)^{1/2}}{m-(m^2-4a^2c^2)^{1/2}}\right)\right]\right\}^{-1}.$$

This formula is advantageous in that the capacitance of the system when the cylinders are concentric is $[2\log_e(b/a)]^{-1}$ statfarads per cm length. Hence the second term of the expression is a correction term for the eccentricity of the cylinders. Thus the effect of eccentricity on the capacitance of a cylindrical condenser is directly determined.

(c) The substitution in (7) may also be made as follows:

$$C=\left\{2\log_e\left[\frac{b}{a}\times\frac{a^2}{b^2}\times\frac{b(m'/2bc+((m'/2bc)^2-1)^{1/2})}{a(m/2ac+((m/2ac)^2-1)^{1/2}}\right]\right\}^{-1}$$

$$=\{2[\log_e(m'/2bc+((m'/2bc)^2-1)^{1/2})-\log_e(m/2ac+((m/2ac)^2-1)^{1/2})]\}^{-1}$$

$$=\{2[\cosh^{-1}(m'/2bc)-\cosh^{-1}(m/2ac)]\}^{-1}. \tag{12}$$

Hence the capacitance of eccentric cylindrical condensers varies inversely as the difference of two hyperbolic angles.

Because of the use of the positive signs in (8) and (9), the value of the capacitance determined by (12) is negative.

A. E. Kennelly[4] has derived the equation for the capacitance in a form which is quite similar to (12).

As c approaches zero, each of the two hyperbolic angles in (12) approaches infinity, but their difference always remains finite. With decreasing values of c, this difference increases at a diminishing rate, approaching as a limit a constant value corresponding to the capacitance of the cylinders when they become concentric.

(d) Eq. (12) may be further simplified. From (8) and (9),

$$\frac{p'}{p}=\frac{(1/2c)[m'-(m'^2-4b^2c^2)^{1/2}]}{(1/2c)[m-(m^2-4a^2c^2)^{1/2}]}.$$

By expanding, $m'^2-4b^2c^2=m^2-4a^2c^2$. Hence,

$$\frac{p'}{p}=\frac{m'-(m^2-4a^2c^2)^{1/2}}{m-(m^2-4a^2c^2)^{1/2}}\times\frac{m+(m^2-4a^2c^2)^{1/2}}{m+(m^2-4a^2c^2)^{1/2}}=\frac{mm'+(m'-m)(m^2-4a^2c^2)^{1/2}-(m^2-4a^2c^2)}{4a^2c^2}.$$

Expanding m and m',

$$\frac{p'}{p}=\frac{(b^2+a^2-c^2)+[(b^2+a^2-c^2)^2-4a^2b^2]^{1/2}}{2a^2}=\frac{b}{a}\left\{\frac{b^2+a^2-c^2}{2ab}+\left[\left(\frac{b^2+a^2-c^2}{2ab}\right)^2-1\right]^{1/2}\right\}.$$

Substituting in (7),

$$C=\{2\log_e[\beta+(\beta^2-1)^{1/2}]\}^{-1}, \quad (13)^5$$

where $\beta=(b^2+a^2-c^2)/2ab$. Hence,

$$C=[2\cosh^{-1}\beta]^{-1}. \tag{14}$$

In the foregoing analysis, the capacitance has been given in statfarads per cm length with vacuum as the dielectric. With a dielectric whose permittivity is κ, the microfarads per 1000 ft. are obtained by multiplying by $3.388\cdot10^{-2}\cdot\kappa$; likewise microfarads per mile are obtained by multiplying by $17.89\cdot10^{-2}\cdot\kappa$.

As an example of the application of (14), let $b=2$ cm; $a=0.5$ cm; $c=1.0$ cm; and $\kappa=1.0$.

The calculated capacitance is 0.5686 statfarad per cm length and the capacitance, when the cylinders are concentric, is 0.3606 statfarad per cm length. The ratio of the capacitance of this

[4] A. E. Kennelly, *The Linear Resistance between Parallel Conducting Cylinders in a Medium of Uniform Conductivity.* Proc. Am. Phil. Soc. **XLVIII** (1909).

[5] Alexander Russell gives Eq. (13). Reference 1, 1904 edition, page 104.

particular eccentric arrangement to that of the concentric arrangement is 1.30.

The Potential Gradient

Pender and Osborne[6] have derived the following Eq. (15) giving the potential gradient at the surface of either of the cylinders of a condenser consisting of two equal parallel cylinders. The cross section of such a condenser is shown in Fig. 2. The radius of each cylinder is a cm. The distance CC' between the axes of the cylinders is D cm, and the distance between the inverse points A and B is d cm.

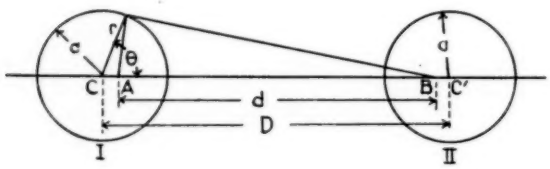

Fig. 2. Parallel equal cylinders and inverse points.

The potential gradient at the surface of either cylinder at P, the intersection of any radius r, is given by

$$\partial V/\partial r = 2Qd/[\kappa a(D-2a\cos\theta)], \qquad (15)$$

where Q is the charge per cm length, κ is the dielectric constant, and θ is the angle which the radius r makes with line CC'. Eq. (15) is the polar equation of an ellipse with the origin at one of the foci.

So far as any effect on cylinder (I) (Fig. 2) is concerned, the charge on (II) may be assumed as being concentrated uniformly along the axis corresponding to the inverse point B. This system becomes analogous to that of Fig. 1, since so far as any effect on the inner cylinder is concerned, the charge on the outer cylinder may be assumed to be concentrated along the axis corresponding to the inverse point B. Hence, (15) is applicable to the system shown in Fig. 1. It only remains to convert the parameters Q, d and D into those corresponding to the system shown in Fig. 1.

[6] Harold Pender and Harold S. Osborne, *The Electrostatic Capacity between Equal Parallel Wires.* Elec. World **56**, 667 (1910).

Referring to Figs. 1 and 2, from (1)

$$BC\times CA = a^2,$$
$$(d+p)p = a^2,$$

where p in Fig. 2 equals CA

$$d = (a^2-p^2)/p \qquad (16)$$

where $d=AB$ in Fig. 1.

In Fig. 2, $D=d+2p$. Hence,

$$D = (a^2+p^2)/p. \qquad (17)$$

Substituting (16) and (17) in (15),

$$\frac{\partial V}{\partial r} = \frac{2Q}{\kappa}\,\frac{a^2-p^2}{a(a^2+p^2-2ap\cos\theta)}, \qquad (18)$$

$$Q = CE, \quad \text{where} \quad E = V_1 - V_2.$$

C is most conveniently given by (14), although any of the other Eqs. (10), (11) and (12) may equally well be used.

Hence

$$Q = \frac{\kappa E}{2\cosh^{-1}\beta} = \frac{\kappa E}{2\cosh^{-1}[(b^2+a^2-c^2)/2ab]} \qquad (19)$$

and

$$\frac{\partial V}{\partial r} = E\,\frac{a^2-p^2}{a(\cosh^{-1}\beta)(a^2+p^2-2ap\cos\theta)} \qquad (20)$$

$$= E\,\frac{a^2-p^2}{ar_1^2(\cosh^{-1}\beta)}. \qquad (21)$$

Hence the potential gradient varies inversely as the square of the distance of the point P from the inverse point A.

For example, if $a=0.5$ cm; $b=2$ cm; $c=1$ cm; and $E=10{,}000$ volts, $p=0.094$ cm, and from (20),

$$\frac{dV}{\partial r} = \frac{10{,}000(0.25-0.0088)}{0.5(\cosh^{-1}1.625)(0.25+0.0088-0.094\cos\theta)} \text{ volts per cm}$$

$$= 48{,}100/(2.755-\cos\theta) \text{ volts per cm.} \qquad (22)$$

The maximum gradient occurs when $\theta=0$ and is equal to 27.4 kv per cm; the minimum gradient occurs when $\theta=180°$ and is equal to 12.8 kv per cm. The corresponding value of the potential gradient with concentric cylinders is 14.42 kv per cm.

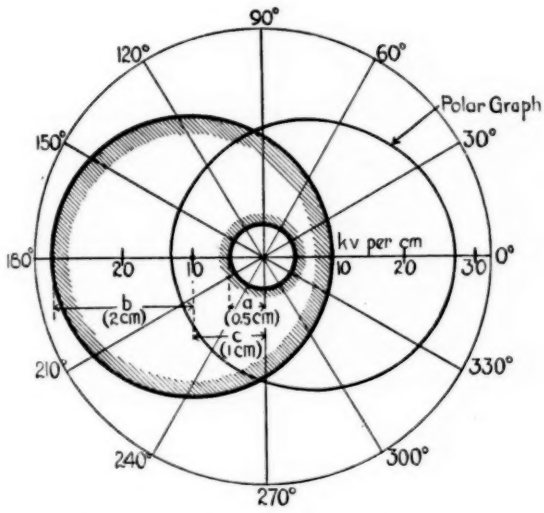

FIG. 3. Polar diagram of potential gradient.

Fig. 3 shows a polar graph of the potential gradient represented by (22).

THE POTENTIAL GRADIENT AT ANY POINT WITHIN THE DIELECTRIC

Let it be desired to determine the potential gradient at any point P_1 within the dielectric of an eccentric cylindrical condenser, Fig. 4. As in Fig. 1, C is the center of the inner cylinder whose radius is a. C' is the center of the outer cylinder whose radius is b and A and B are the inverse points of the system.

Draw $P_1C=r$, P_1A and P_1B; let θ be the angle between $P_1C=r$ and CB. If P_1 is determined by the polar parameters r and θ, P_1A and P_1B are readily determined trigonometrically, since $CA=p$ and $AB=d$ are already known. Draw P_1C_1 such that $<C_1P_1A=<P_1BA$, C_1 lying on BA extended. C_1 is the center of the equipotential circle passing through P_1 and C_1P_1 is its radius a_1. Let M_1 be the intersection of the circle with AB; also let $C_1A=p_1$.

Triangles C_1P_1A and C_1P_1B are similar, and

$$C_1A/C_1M_1=p_1/a_1=C_1M_1/C_1B,$$

$$p_1=a_1^2/(C_1A+AB)=a_1^2/(p_1+d). \quad (23)$$

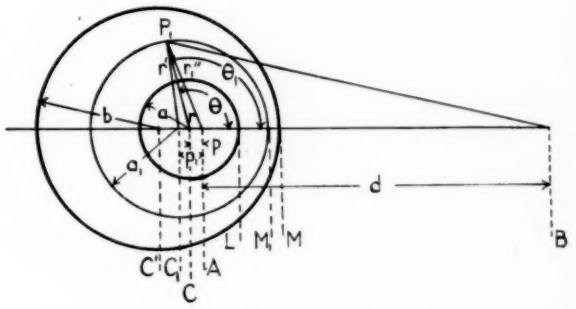

FIG. 4. Potential gradient within dielectric of eccentric cylindrical condenser.

It also follows that

$$C_1A/C_1M_1=p_1/a_1=AP_1/BP_1. \quad (24)$$

Solving (23) and (24) simultaneously,

$$p_1=d/[(BP_1/AP_1)^2-1], \quad (25)$$

$$a_1=(d(BP_1/AP_1))/[(BP_1/AP_1)^2-1]. \quad (26)$$

The angle θ_1 between the radius P_1C_1 and C_1A, is readily determined since P_1A, $P_1C_1=a_1$ and $C_1A=p_1$ are all known.

Substituting (19) in (18), making $a=a_1$, $p=p_1$ and $\theta=\theta_1$ corresponding to point p_1,

$$\frac{\partial V}{\partial r'}=\frac{a_1^2-p_1^2}{a_1(\cosh^{-1}\beta)(a_1^2+p_1^2-2a_1p_1\cos\theta_1)} \quad (27)$$

$$=E\frac{a_1^2-p_1^2}{a_1r_1''^2[\cosh^{-1}\beta]},$$

where $r_1''=AP_1$.

For example, under the conditions from which (22) was obtained, with $r=1.4$ cm, $\theta=135°$, computation gives $AP_1=r_1''=1.467$ cm; $BP_1=3.785$ cm; $p_1=0.4537$ cm; $a_1=1.171$ cm; and $\theta_1=122.6°$.

$\partial V/\partial r=4.335$ kv per cm as compared with 13.89 kv per cm at the surface of the conductor at its intersection with the same radius r.

The author is indebted to Dean H. E. Clifford of The Harvard Engineering School for his many helpful suggestions in the preparation of this paper.